DESIGN AND MODELING OF A NON-THERMAL PLASMA REACTOR FOR CO_2 DISSOCIATION.

A THESIS SUBMITTED TO
THE BOARD OF CAMPUS GRADUATE SCHOOL OF
MIDDLE EAST TECHNICAL UNIVERSITY, NORTHERN CYPRUS CAMPUS
BY

HUMAYUN AHMED

IN PARTIAL FULFILLMENT OF THE REQUIREMENTS
FOR
THE DEGREE OF MASTER OF SCIENCE
IN
SUSTAINABLE ENVIRONMENT AND ENERGY SYSTEMS PROGRAM

JANUARY 2017

Approval of the Board of Graduate Programs

_____

Prof. Dr. Oya Yerin Güneri
Chairperson

I certify that this thesis satisfies all the requirements as a thesis for the degree of Master of Science

_____

Assist. Prof. Dr. Carter Mandrik
Program Coordinator

This is to certify that we have read the thesis and that in our opinion it is fully adequate, in scope and quality, as a thesis for the degree of Master of Science.

_____

Assist. Prof. Dr. Onur Taylan
Supervisor

Examining Committee Members:

Assist. Prof. Dr. Onur Taylan	Mechanical Engineering METU NCC	_____
Assist. Prof. Dr. Dizem Arifler	Physics METU NCC	_____
Assist. Prof. Dr. Feyza Kazanç	Mechanical Engineering METU ANKARA	_____

I hereby declare that all information in this document has been obtained and presented in accordance with academic rules and ethical conduct. I also declare that, as required by these rules and conduct, I have fully cited and referenced all material and results that are not original to this work.

Name, Last name : Humayun Ahmed

Signature : _____

ABSTRACT

Modeling and Design of a Non-Thermal Plasma Reactor for CO_2 Dissociation

Ahmed, Humayun

MSc., Sustainable Environment and Energy Systems Program

Supervisor: Assist. Prof. Dr. Onur Taylan

January 2017, 94 pages

The requirement of energy constantly increases with time, and one of the major sources of energy is fossil fuels which release carbon dioxide upon combustion. Environmentally, CO_2 is a greenhouse gas which has had a tremendous impact on the Earth's climate over the last few decades and the urges serious mitigation methods for the long-term sustainability of the Earth's climate and ecosystem. One mitigation method is the dissociation of CO_2 to produce synthesis gas which can be used to produce alternative hydrocarbon fuels. There have been studies investigating the use of plasma reactors for synthesis gas production but experimentation has proven to be resource and time consuming. Hence, this study focuses on modeling the dissociation of carbon dioxide in non-thermal plasma reactors via a one-dimensional fluid approximation and a zero-dimensional kinetics analysis. A sensitivity analysis on the results is conducted by using different collision cross-section data for the electron impact dissociation of CO_2. The results show the spatial distribution of electrons depends upon electron attachment, ionization and electronic excitation of CO_2 primarily, and addition of carrier gases such as Argon and Xenon and their effects on the shape of distribution.

Keywords: Non-thermal Plasma, Carbon dioxide dissociation

ÖZ

CO_2 Ayrışması için Termal Olmayan Plazma Reaktörünün Modellemesi ve Tasarımı

Ahmed, Humayun

Yüksek Lisans, Sürdürülebilir Çevre ve Enerji Sistemleri Programı

Danışman: Yrd. Doç. Dr. Onur Taylan

Ocak 2017, 94 Sayfa

Enerji ihtiyacı zamanla sürekli olarak artmaktadır ve temel enerji kaynaklarından birisi yanma sonrasında karbon dioksit (CO_2) salan fosil yakıtlardır. Sera gazı olan CO_2 , son birkaç on yılda dünya iklimi üzerinde çevresel olarak olumsuz etkiler yaratmakta ve iklim ve ekosistemin uzun vadeli sürdürülebilirliği için ciddi yöntemlerin gerekliliğini ortaya çıkarmaktadır. Bir yöntem, alternatif hidrokarbon yakıtları üretmek için kullanılabilecek sentez gazı üretmek için CO_2'yi ayrıştırmaktır. Bu yöntem için plazma reaktörlerinin kullanımına yönelik araştırmalar yapılmış ancak deneysel yapılan araştırmalar hem kaynak hem de zaman kayıplarını beraberinde getirmektedir. Bu sebeple, bu çalışma termal olmayan plazma reaktördeki karbon dioksit ayrışmasının modellemesini üzerine odaklanmaktadır. Çalışma kapsamında iki temel model kullanılmıştır; akışkanlar yaklaşımı içeren tek boyutlu model ve sıfır boyutlu reaksiyon kinetiği modeli. Elektron çarpışmasına dayalı CO_2 ayrışması için farklı çarpışma kesit verileri kullanılarak sonuçlar üzerine bir duyarlılık analizi yapılmıştır. Çalışma sonuçları, elektronların reaktör içerisindeki mekansal dağılımının öncelikle elektron bağlanmasına, iyonlaşmasına CO_2'nin elektronik uyarılmasına bağlı olduğunu göstermiştir. Ayrıca, Argon ve Xenon gibi taşıyıcı gazların kullanılması da elektron dağılım şeklinin değişmesine sebep olduğu sonucuna varılmıştır. Sıfır boyutlu reaksiyon kinetiği modeli de kütlesel olayların etkilerini benzetimler aracılığıyla açığa çıkarmış ve CO_2 ayrışmasını niteliksel olarak incelemeye olanak sağlamıştır.

Anahtar Kelimeler: Termal Olmayan Plazma, Karbondioksit Ayrışması

DEDICATION

To my Parents, Wife and Brothers

ACKNOWLEDGMENTS

I thank God Almighty for providing me with ability to pursue higher studies.

I would like to thank my Supervisor Assist. Prof. Dr Onur Taylan who has supported and guided me throughout the completion of my thesis. His patience and comments helped make this study a possibility.

I would also like to thank all of colleagues that supported me throughout the process. My roommate Fahad Haneef and friends Obaidullah Mohiuddin, M. Saleh Rashid, Loiy- Al-Ghussain and my Seniors S.M. Hassan Ali, Arsalan Tariq and Fassahaullah Qureshi.

I would like to express my eternal gratitude towards my beloved parents, brothers and wife for their unconditional love and support.

The support of Middle East Technical University Northern Cyprus Campus, Campus Research Fund (project no.: BAP-16-YG-3) is gratefully acknowledged.

TABLE OF CONTENTS

LIST OF TABLES

LIST OF FIGURES

LIST OF ABBREVIATIONS

NTP	Non-thermal plasma
CCP	Capacitively coupled plasma
DBD	Dielectric barrier discharge
RF	Radio-Frequency
MHCD	Micro Hollow Cathode Discharge

CHAPTER 1

INTRODUCTION AND AIM OF THE STUDY

1.1 Introduction

Energy plays a key role in governing the technological progress of any nation. Since the industrial age, the surge in consumption of fossil fuels to meet the demands of the populace and industry has led to the onset of global warming. A natural heating phenomena that has been enhanced due to excess CO_2 in the atmosphere, trapping long-wavelength radiation and generating a heating effect. This led the scientific community to discover renewable and clean energy sources that could help in the abatement of global warming. Solar and wind energy show immense potential in providing for global energy needs.

However, the problem with solar and wind energy is the highly intermittent nature of the resource. The availability quality of solar energy is subject to the presence of a clear sky and location, even though extra-terrestrial irradiance can be determined for any latitude and longitude using well established analytical and empirical relations [1]. Wind energy is highly location specific and unpredictable in short time scales with varying intensity. This means that systems storage systems should be utilized to provide power when renewable resources fall short.

Storage in the form of readily available chemical fuels is becoming a possibility. The use of plasma can enable degradation of unwanted chemical such as methane and carbon dioxide into a more useful mixture of synthesis gas ($CO + H_2$). This can then be utilized to make value added chemicals or simply synthetic fuel [2, 3, 4]. In the latter case, this process can effectively close the carbon cycle and mitigate increasing CO_2 concentration in the environment. In the long run, complete replacement of current energy technology with renewable power might be plausible but the power delivered by chemical fuels remains unrivaled for several applications.

The applications of plasma assisted processes require a strong understanding of the underlying physical and chemical phenomena. Dissociation of chemical compounds via electrical discharges in plasma has gathered interest over the years. Carbon dioxide and hydrocarbon breakdown using plasma is a relatively new field of study. The full kinetics of the numerous complex reactions are still not completely understood. Hence, work on increasing dissociation rate whilst minimizing input power is a key goal but requires thorough numerical and experimental analysis.

Several experimental studies focusing on hydrocarbon reforming, chemical compound dissociation (pollution reduction) have been conducted with different objectives. However, very few numerical studies exist in detailing the phenomena of CO_2 breakdown in a plasma. Experimental approaches require resources and are limited in the number of scenarios that can be analyzed. The possibilities are too many for any single experiment to cover.

1.2 Aims and Objectives

The study aims to analyze CO_2 dissociation via two different models. The first model is a simple model one-dimensional which can enhance understanding of phenomena that rely on the distribution of electrons, mean energy and active species to aid in designing and optimizing the non-thermal plasma (NTP) reactor. The second is a zero-dimensional kinetics model.

A validation of CO_2 dissociation is difficult at this stage, firstly, due to the lack of a simple experimental setup and the complexity that arises from incorporating a large set of reactions but qualitative trends can be captured. The core objectives are summarized below,

- To examine one-dimensional spatial distribution of pure CO_2 dissociation and CO_2/Ar, CO_2/Xe mixtures in a capacitively coupled plasma discharge under conditions validated by a Helium discharge model.

- To explain qualitatively and quantitatively the distribution of the species and rate of reactions in the NTP and present design recommendations for CCP reactors.

- To analyze the sensitivity of the results when considering different published CO_2 electronic excitation cross-sections leading to dissociation into neutral CO and O fragments.

- To examine the effects of different assumptions such as, assuming a collision cross-section data, reduction of activation energy for molecular interactions on the spatial distribution of species and spatial distribution of reaction rates in the NTP.

- To highlight the limitations of the zero-dimensional modeling for dissociation of CO_2. Specifically, the sensitivity of the results to assumptions of power density and set of reactions. Results are compared by showing the difference in CO_2 conversion fraction and conversion efficiency.

CHAPTER 2

LITERATURE REVIEW

Plasma is a quasi-neutral ionized gas. It is generated when the gaseous mixture is provided enough energy such that the electrons are able to escape from the atoms. A sufficient number of free electrons and ions are required before the mixture is able to fully sustain itself. A special class of plasmas, "non-thermal/non-equilibrium" (NTP) plasmas are formed when the free electron, ion and neutral gas temperatures are not in thermodynamic equilibrium. However, given sufficient time, the collisions between electrons and heavier particles (gas atoms and ions) will raise the gas temperature.

Dissociation of CO_2 is garnering interest due to its potential use in hydrocarbon reforming, lasers and synthesis gas formation. The concept of solar renewable fuels is an innovative way to mitigate CO_2 emissions [5]. Several independent studies, not primarily focused on CO_2 mitigation, have been conducted since the 1970's and 1980's [6]. Understanding of CO_2 dissociation under several non-equilibrium conditions has rapidly progressed but due to a lack of fast computational resources during 1980's, the solution to the fluid equations involving pure CO_2 was not conducted. The focus was to determine dominant reaction pathways that contribute to high energy conversion efficiency.

In the next sections, various experimental studies are outlined with key findings that stimulate the interest into CO_2 dissociation to produce useful compounds via NTP. The purpose is to show the promising outcome and potential in utilizing NTP for converting CO_2 into synthesis gas, enhancing methane reforming or cracking larger hydrocarbons.

2.1 Pure CO_2 Studies

There has been significant effort in exploiting the useful properties of non-equilibrium plasmas [7]. Since the overall temperature of the plasma is close to room temperature, it can be effectively utilized. In industrial applications, it is common to see noble gas

plasmas (Helium, Argon, Xenon etc.). However, the composition of the plasma is an important factor governing its behavior, meaning a Helium or Argon plasma will display different discharge phenomena under the same conditions as opposed to a CO_2 plasma. It is known that modelling Argon or Helium requires few reactions that mainly comprise a single ionization reaction, electronic excitation and elastic collisions. [8].

CO_2 chemistry is more complex as it involves dissociation into fragments that can combine to form new species, for example ozone (O_3) and oxygen (O_2) in ground neutral state or charged ionic states etc. Hence, a large number of chemical reactions that comprise majority, if not all, of the chemical species formed need to be considered if modeling efforts are to be considered accurate. Experimental approaches on the other hand provide data on bulk phenomena such as electrical discharge characteristics (current waveforms, charge deposited etc.).

Studies dedicated to examining CO_2 dissociation under various conditions are lacking, many experimental but not enough numerical efforts are dedicated to this purpose. Recent interest in capturing solar energy in so called solar fuels has brought about a focus on pure CO_2 dissociation under various conditions. In those studies, as mentioned in this chapter, several aspects still require exploration (collision cross-sections, computational efficiency of mathematical models etc.) and experimental conditions not capturing a wide range of conditions.

Recently, the catalytic properties of non-thermal plasma (NTP) have opened doors into its potential use in generating carbon neutral processes [9]. Several studies have been conducted examining the dissociative properties in various gas mixtures [10, 11, 12]. Several reactor designs have been proposed and have varying efficiencies and conversion rates at different operating conditions. Gliding Arc discharges have been experimentally shown to provide high conversion rates of carbon dioxide and methane mixtures at low costs [13, 14, 15]. The plasma vortex configurations affect the energy efficiency. A maximum thermodynamic efficiency of 43% is attainable through reactor design and exploiting the energy efficient pathways in CO_2 breakdown [16]. The energy efficient

pathways, however, are mainly vibrationally excited modes of CO_2. This leads to significant heating which can speed up reformation of CO_2 from fragment CO and O and O_2 molecules. Fast quenching rates are required to suppress this reformation in order to maximize energy conversion efficiency.

Another class of reactors in which the conducting electrodes are covered with either a thick or thin dielectric is termed as Dielectric Barrier Discharges (DBD). [17] provides a detailed explanation of the typical discharges encountered in a DBD. Figure 1 shows a typical cylindrical DBD schematic [18].

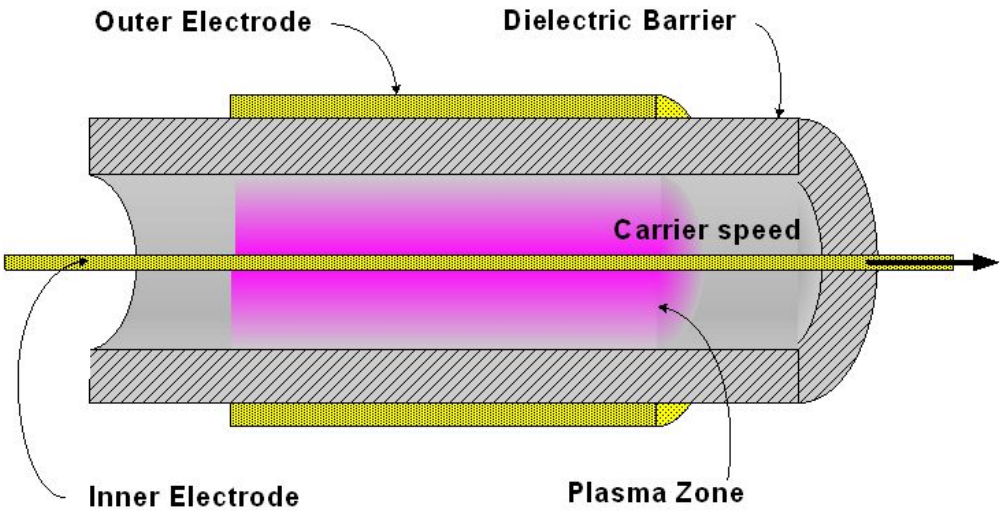

Figure 1. A typical cylindrical DBD reactor. The discharge gap is the radius of the annulus [18].

If the plasma is exposed to a catalyst at different temperatures, the selectivity of products (formation of CO mainly) can be positively affected to increase CO_2 dissociation even at high temperatures [18, 19, 20]. The gas temperatures can be raised well beyond room temperatures (greater than 673 K) and CO_2 selectivity increases as soon as the plasma was introduced to the catalyst such as La_2O_2.

Since CO_2, industrially, is not released in a pure form as combustion efficiencies are less than 100. It can be accompanied by unburnt hydrocarbons such as methane. Experimental

evidence shows that, both, CO_2 breakdown and hydrocarbon reforming of methane can be enhanced using a DBD plasma. CO_2/CH_4, in varying ratios, can be used to influence conversion into higher hydrocarbons [21, 22, 23].

An early study [24] analyzing the effect of increasing number of reactors (numbering-up) or increasing geometry (diameter and length, scaling-up) for CO_2 decomposition. It is the first study to recommend numbering up for high conversion rates and scaling up for high power efficiency. Although not directly stated, a compromise between conversion and power efficiency is clearly observed.

A review of CO_2 dissociation techniques via NTP and compares the existing technologies in terms of energy and conversion efficiency [25]. In order for NTP or TPs to be competitive in the industry, several factors influencing the conversion need to be optimized and a significant leap in energy and molar conversion has to be reached. This presents a dilemma, since increasing flow rate negatively affects the energy and conversion efficiency.

Design criteria are not fully established for dissociation of CO_2. A new design in high flow rate DBD reactors [26] observes the effect on conversion efficiency and mole fraction of CO_2 and methane (CH_4) with Argon/Helium as the carrier gas in a dielectric barrier discharge reactor (DBD). The reactor was designed to study high flow rates, with a maximum diameter of 34 mm and length of 100 mm. The electrodes were made of copper and the cathode was covered with Alumina as the dielectric. Hence, typically long reactors consist of a few centimeters.

Several numerical and experimental approaches where the numerical model relies on the specific experiment are also found. The conversion of CO_2 in a packed bed DBD reactor [27]. To account for the packing with beads of different materials, the reactor diameter was kept large (22 mm). The numerical analysis consisted of a 0-D model with known reaction rates obtained from other studies [28]. A COMSOL 2-D model was solved with Helium plasma to understand the change in electric field due to the packing. A point to note is that, intricate and highly sophisticated models would take weeks to simulate for a

few voltage cycles as pointed out by the authors, hence Helium was used to gain insight into the electric field strength near the beads (sheath regions) and towards the bulk of the plasma. The electric field was noticeably enhanced close to the beads due the formation of sheath regions.

Similarly, effect of process parameters (input power, flow rate, discharge length etc.) on CO_2 dissociation in a DBD reactor using design of experiment method [29] is another approach that avoids complex simulations. A non-linear regression (quadratic) was performed to relate the variables. The experimental setup consisted of a variable discharge length of 90 to 150 mm, width 2.5 mm, flow rate of pure CO_2 between 15-45 ml/min, maximum voltage of 10 kV at 10 kHz frequency. They concluded that increasing the applied voltage at a fixed frequency increases the electron density in the discharge gap.

2.2 CO_2 Dissociation in Mixtures

It has also been of interest to examine and understand the process of reforming methane into larger hydrocarbons and improve the conversion yield of CO_2 by adding noble gases such as Argon and Helium. The primary purpose of such experimental approaches is to simply increase the energy efficiency or yield, not just to produce synthesis gas. Hence, different mixtures of varying concentrations, input conditions, discharge parameters (current-voltage waveform) and reactor type have been investigated in the previous years.

Methane conversion is known to be enhanced in a DBD when CO_2 is added to the mixture. This leads to the production of synthesis gas and larger hydrocarbon chains whilst minimizing carbon deposition in the reactor. The selectivity of the products depends upon the feed ratio of CH_4/CO_2, power applied and catalyst used [30]. Later, the influence of a catalyst on CO selectivity is studied against varying temperatures, input power and feed ratios. CO selectivity is increased in the presence of a catalyst at high temperatures [18].

Although not a pure CO_2 mixture, diesel exhaust decomposition using DBD [31] provides useful insight. Discharge power is related to the voltage level and applied frequency. It

was shown conclusively, that CO_2 selectivity at high voltages exceeding plasma formation threshold (break-down voltage) have a greater impact on CO_2 dissociation as opposed to the applied frequency. At low voltages both frequency and voltage levels have a strong impact on CO_2 degradation. Although the study considered only 4 key reactions involving the breakdown of CO_2, the point was to illustrate that higher voltage leads to favoring of electron impact dissociation.

An innovative mechanism to produce methane using water assisted CO_2 dissociation is investigated by [3]. This is the first study to detect methane formation via pure CO_2 gas over a water film in a pulsed corona discharge. The benefit was removal of CO_2 and production of methane which can be stored. This presents an alternative energy storage mechanism similar to synthesis gas.

In the studies mentioned above, effect of input power waveforms was not exclusively highlighted.

The influence of different input power waveforms on dissociation characteristics of a CO_2-Helium mixture in a DBD reactor has also been investigated [32]. There is an increase in dissociation when using an AC signal as opposed to a pulsed discharge commonly used in DBD. This was attributed to the vibrational excitation of CO_2 in AC signals, which is more efficient. Additionally, reactor wall temperatures were measured and found to be lower in a pulsed discharge and higher in AC powered reactors.

Synthesis gas formation from a CH_4/CO_2 mixture under different applied voltage waveforms (AC or pulsed) shows that the products are affected by the choice of the waveform [33]. A pulsating waveform results in higher values of discharge current and discharge power, which is proportional to an increase in plasma conductivity. However, an AC sinusoidal waveform results in higher energy conversion efficiency and specific energy. If the applied power is the same then a larger fraction goes into dissociation the mixture in the case of an AC waveform but because the delivered power was always lower compared to a pulsed waveform, the product selectivity was lower.

Experimental approaches towards understanding the mechanisms involved in NTP reactors are effective if a specific situation is being studied. The major drawback is that the number of scenarios that can be verified depends directly upon the resources available. Numerical studies in this scope have evolved over the years and allow for an infinite number of scenarios to be studied but with reduced accuracy.

There are typically three unique methodologies adopted in literature that are used to model NTP discharges in various reactors. Discussed briefly in Section 2.3, they are Monte-Carlo simulation, solution to the Boltzmann Equation and the Fluid approximation of a plasma.

2.3 Monte-Carlo Simulations

Plasma is an ensemble of charged species that behave in a manner that negates the effect of additional charges thereby maintaining quasi-neutrality. If the velocity of every species is known, as opposed to a velocity distribution function, then an accurate estimation of the properties of a plasma can be made. In Monte-Carlo simulations, each electron and particle is given a random trajectory and given the probability of collision events, the position and velocity can be solved for using newtons equations of motion. The set of governing equations comprise simply (in one dimension),

$$m\frac{d^2x}{dt^2} = \vec{E}q \tag{1}$$

$$\frac{\partial^2 \emptyset}{\partial x^2} + \frac{e}{\varepsilon}(n_i - n_e) = 0 \tag{2}$$

2.4 Boltzmann Distribution Function

The solution to the Boltzmann distribution function gives the electron energy distribution function which can provide the rate constants for the various reactions occurring in the NTP [34]. If the equilibrium electron number density is known, then rates of reaction can be determined and solved in a zero-dimensional kinetics model.

2.5 Magneto-Hydrodynamic Equations (Fluid Equations)

The fundamental conservations laws can be applied to plasmas to obtain partial differential equations that describe the plasma as a fluid under electromagnetic fields. These equations can be obtained by conducting a mass, force and energy balance on an element [35] or by taking velocity moments about the Vlasov (Boltzmann) equation. The zeroth order moment gives the mass conservation; the first order moment gives the momentum conservation and the second order gives energy conservation. These three moments coupled with Maxwell's laws governing behavior of charges in free space provide a self-consistent description of a plasma [36, 37]. The set of equations generally include the effects of electric and magnetic fields. This form is referred to as the Magneto-Hydrodynamic Equations (MHD). In the absence of an applied magnetic field, the equations are greatly simplified and are reduced to the fluid approximation coupled with Poisson's Equation for the electric potential distribution.

If ions, electrons and neutrals (excited species) are grouped together in a fluid element, then it is referred to as a single fluid approximation to the MHD equations. If each species is treated separately, then it is a multi-fluid approximation. However, regardless of the choice, the inherent lack of accuracy due to lumping of species within a single element is always present (Plasma theory differs greatly from single particle physics under electromagnetic fields). Additionally, the assumption of a Maxwellian distribution is assumed for species. This may hold in many situations but electrons can greatly deviate from this distribution. Figure 1, shows a Maxwellian distribution function for electron energy at three mean electron energies. Notice that the peaks correspond to the mean energy.

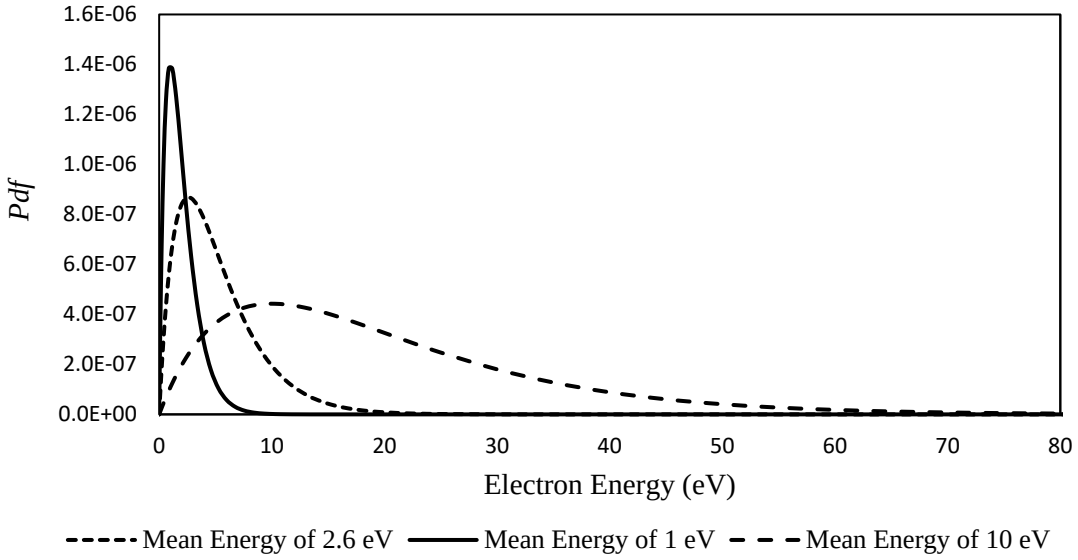

Figure 2. Maxwellian distribution function of electron energy (EEDF) for three different mean energies.

The source and sink terms occurring in the mass and energy conservation equations are functions of the energy distribution of the species, cross-section of the target particle and population density of the incident species. There are several expressions widely used in literature for expressing the reaction rate. The Arrhenius form expresses the reaction rate in terms of the population density and species temperature, shown in Equation (3).

$$R = A\exp(-\frac{E_a}{kT}) \tag{3}$$

where, A is the pre-exponential factor and E_a is the activation energy of the collision or threshold energy, k is the Boltzmann constant and T is the electron temperature in K.

While a more exact formulation would involve the above-mentioned variables in a single integral. This is another limitation of the fluid theory. The electron energy distribution function has to be known before reaction rates can be evaluated or source terms expressed. An assumption made at this point is to consider the initial distribution to be Maxwellian and determine the deviation via an iterative process.

The fluid theory is popular as it is relatively easy to solve compared to the Kinetic theory and requires significantly less storage compared to Monte-Carlo methods.

In this study, the multi fluid approximation is used to examine the effect on dissociation rates of several compounds such as CO_2, Argon, Helium and their mixtures. The effect of varying the applied voltage frequency, reactor diameter, gas temperature on the reaction rate in the reactor is examined.

2.6 Dissociation Reactions

Every molecular compound can be 'broken' into other molecules or atoms if sufficient energy per mole of substance is provided. The bond energy in the molecule, which holds the compound together can be overcome by several collision pathways which lead to dissociation. The key is to dissociate the substance with high energy efficiency. Indeed, not all the energy supplied to the substance goes into dissociating it (breaking bonds). A significant fraction simply heats the bulk gas. The more stable the bond and the more energy is required to split the parent molecule.

Carbon dioxide is stable at 2000℃ at atmospheric pressure [38] which means through ordinary reforming methods it takes tremendous heat to raise the temperature and initiate decomposition.

Plasma assisted dissociation is a very efficient process for breaking bonds in compounds. The presence of highly energetic species in the plasma (ion, electrons and excited neutrals) can overcome the bond energy upon a single or multiple stepwise collisions. A brief introduction into the types of collision specific to plasmas is provided in this section. A detailed explanation and well-referenced text can be found in [39, 40]

A collision in the classical world is easy to visualize, and generally can be said to have occurred when the colliding bodies are in contact. This requires the colliding bodies to have a geometry. However, when dealing with atomic and sub-atomic particles, a collision

is not easily defined. A particle can influence another even at a large distance (Coulomb potential). Hence, some collision parameters have to be defined.

Cross-section: The total blocking area presented to the incoming particle (test particle). The field particle is the one that is subjected to a flux of test particles. Mathematically, cross-sections are defined as:

$$Q = \frac{v}{\Gamma} \tag{4}$$

where, v is the rate at which the test particles are interacting with a single field particle in 1/s, and Γ is the incident flux of test particles in $1/m^2s$. An example of a field particle would be a ground state CO_2 molecule, while a test particle could be an electron.

If one thinks classically and approximates an atom to be a sphere with radius equal to the atomic radius, then the so called hard-sphere cross-sections are obtained but such cross-sections are only helpful when dealing with ground state neutral to neutral collisions. Almost any deviation from the ground state produces different cross-sections. Analytical expressions are available for several types of collisions such as elastic, ionization etc. Thes expressions use a Maxwellian form of the energy distribution and a differential form for the cross-section.

Energy distribution function: A function describing the probability of obtaining a particle with a particular energy value (EDF). In non-thermal plasmas the heavier species (ions, neutrals and excited atoms/molecules) are usually at a temperature much lower than the temperature of electrons. Hence, the distribution function is generally ignored when calculating the rate constants for heavier species. For electrons, the energy distribution (EEDF) is quite important as it drives the electron impact reactions. An equilibrium distribution (Maxwellian) is assumed in many of the cases as obtaining an accurate EEDF can be complicated. The influence of random and directed motion (motion in an electric or magnetic field) is significant. In general, random or thermal motion drives the EEDF

towards equilibrium [36] since the energy between two species of equal masses is exchanged efficiently, such as in an electron-electron collision.

There are several collision pathways that lead to dissociation of the parent molecule. In this study, one of the objectives is to arrive at a reliable reduced chemical kinetic model for CO_2. To understand the dominant reactions pathways in CO_2, a brief introduction into the mechanisms is provided and then pathways influencing CO_2 dissociation are considered.

Reaction Types:

Ionization: A molecule is positively ionized when the incident electrons or excited species has energy exceeding the ionization potential for that ionization level. A negative ion is formed when an electron attaches itself to an electronegative atom or molecule. The energy released is referred to as the electron affinity (EA). The process is inelastic as it results in the production of an electron (positive ion) or release of energy (electron attachment, negative ion).

$e + CO_2 \rightarrow 2e + CO_2^+$	Ionization	$\Delta E = -13.80$ eV
$e + CO_2 \rightarrow CO + O^-$	Electron Attachment	$\Delta E = E$ if $E > 3$ eV
$e + CO_2 \rightarrow 2e + CO^+ + O$	Dissociative Ionization	$\Delta E = -19.10$ eV

In a plasma, the above process can occur via several paths. Direct electron impact, stepwise excitation followed by an electron impact, electron attachment and photoionization. The dominant path is difficult to specify in some cases as it depends on the electron density, temperature, species density, etc.

Direct electron impact ionization occurs when the colliding electrons energy exceeds the ionization potential and is the primary source of electron production. In step-wise

ionization, an electron collision with an electronically excited state results in the production of an ion but electronic excitation is slower in low energy plasmas.

Excitation: It is possible for a molecule to resonate to a higher energy level if sufficient energy is imparted in a collision event. The mode of excitation can be vibrational or translational. The excited species is chemically the same as the ground state but can promote other collisional processes such as ionization or dissociation (bond breaking) by reducing the activation energy. The number of excitation levels depends on the mode of excitation (vibrational, electronic, rotational) and molecule itself. A precise understanding of these modes and levels is not within the scope of this study.

In CO_2, dissociation takes place via the formation of an intermediate electronically excited state. If the energy of the incident electron exceeds the threshold energy by a small margin then, dissociation probability is more likely.

Vibrational excitation is due to the elastic nature of C = O bond. The amplitude of vibration increases as the excited state (quantum level) increases. Eventually, the bond energy is exceeded and the bond breaks. It is termed Asymmetric vibration if vibrational amplitudes of both C = O double bonds are different.

Recombination: An electron will be lost in an interaction with a positive ion or conducting surface. The high energy of the electron makes it inefficient in exchanging energy with a heavy particle (ions and neutrals) but it can facilitate dissociative recombination by breaking the molecular ion into other compounds. This is a slow process, since with increasing energy the rate of dissociative recombination decreases owing to the increasing electron thermal velocities.

In mono-atomic gases, such as Argon, Helium or Xenon, the process requires the formation of a dimer ion such as Ar_2^+. This diatomic ion then recombines with an electron via the path mentioned above.

Photo-emissive recombination is slow and three-body recombination in which the third body can be an electron proceeds slower in non-thermal plasmas. It is significant in thermal plasmas where ion and electron temperature are close which gives comparable velocities.

Elastic: A collision in which the kinetic energies of the species is conserved and merely results in distribution of the kinetic energies. It can be shown that the fractional energy transferred by a mass m to a heavier mass M is equal to $\frac{2m}{M+m}$. For CO_2 this ratio is extremely small.

CHAPTER 3

MODELING TECHNIQUES

3.1 Numerical Methods

Simulation of a plasma is performed, with varying accuracy and computation time, via the three main techniques namely, Monte-Carlo Simulations, solution to the Boltzmann Equations and Fluid approximation of a plasma mixture (MHD). In the sections that follow, the multi-fluid approximation is solved to provide a spatial and temporal distribution for a pure CO_2 plasma, so that from an engineering point of view, designs can be later optimized. A detailed two-dimensional simulation is beyond the scope of this study and has yet to be performed by the scientific community in general. This is largely due to the extremely large computation time associated with modeling a large number of chemical species and reactions [41]. Nevertheless, a simplified one dimensional model can be established to qualitatively describe the important mechanisms at this stage.

The solution technique is not dependent on the gas phase chemistry. Since, the composition (number of species) of the plasma merely increases the number of partial differential equations at any given point. It is, however, dependent on the boundary conditions and model constraints.

Mass, momentum and energy balance for electrons and heavy particles (ions and radicals) coupled with Poisson's equation for electric potential distribution. New methods are usually tested against noble gas discharges of Helium or Argon, since they are widely used in the industry and are easier to model.

Several approaches have been taken to solve the fluid equations coupled with Poisson's equation [42, 43, 35, 44]. The set of parabolic and elliptic PDE's are solved in a three-moment approximation either using a fully-implicit (rare) approach or a semi-implicit approach.

Fully implicit approaches are complex to code and sometimes not possible to express mathematically in a usable algebraic form. If the system of equations involves coupling, the complexity increases. A fully explicit expression of the system of equations is computationally attractive but is not preferred. The reason being that apart from the Courant–Friedrich's–Lewy (CFL) condition that limits fully explicit expressions from assuming a large time step in Fluid models. In the fluid approximation of a plasma, the addition of Poisson's equation introduces a Dielectric Relaxation Time which critically limits the stable time step to very small values [45].

A semi-implicit treatment yields the required numerical stability for the solution to progress in time steps that are larger than the classical CFL condition [46].

It is important to have a basic understanding of numerical solution techniques unique to plasma models. This allows wider understanding of the several assumptions made on the model and system of equations.

$$\frac{\partial \mathrm{n_i}}{\partial \mathrm{t}} + \frac{\partial \mathrm{F_i}}{\partial \mathrm{x}} = \mathrm{S_{ij}} \tag{5}$$

$$\mathrm{F_i} = -\mathrm{D_i}\frac{\partial \mathrm{n_i}}{\partial \mathrm{x}} \pm \mu_\mathrm{i}\mathrm{n_i}\frac{\partial \emptyset}{\partial \mathrm{x}} \tag{6}$$

$$\frac{\partial(\epsilon \mathrm{n_e})}{\partial \mathrm{t}} + \frac{\partial \mathrm{F_\epsilon}}{\partial \mathrm{x}} - \mathrm{eF}_e\frac{\partial \emptyset}{\partial \mathrm{x}} = \mathrm{S_{ij}}\Delta\epsilon \tag{7}$$

$$\frac{\partial^2 \emptyset}{\partial \mathrm{x}^2} + \frac{\mathrm{e}}{\varepsilon}(\mathrm{n_i} - \mathrm{n_e}) = 0 \tag{8}$$

$$\mathrm{S_i} = \mathrm{n_1 n_2 k_i} \tag{9}$$

where n_i is the number density of any species in $1/m^3$, F_i is the flux of any species in $1/m^2s$, $\emptyset$ is the electric potential in V, S_{ij} is the source term for species i, reaction j, ϵ is

the mean electron energy in eV, F_e is the energy flux through the element in eV, $\Delta\epsilon$ is the loss or gain of energy during a collision in eV and k_i is the rate constant for the reaction.

The time discretization in the species conservation and electron energy conservation equation is a backward Euler expansion, in its simplest form. Usually, the time step selection is limited by the size of the spatial element. In such a case, a variable order time step methods are employed [47] combined with Newton-Raphson iteration for non-linear equations. The higher order backward difference methods do not necessarily enhance stability and it is shown that above order 7, stability decreases [48]. Hence, the use of numerical methods such as Adams-Bashforth-Molton (ABM) semi-implicit expression for the time may be a starting point for a stable solution because the lowest order ABM scheme uses one fully implicit term and several explicit terms for the dependent variable.

Naturally, the process becomes increasingly complex if advanced numerical schemes are used to evaluate the time derivative. It is, however, not entirely necessary in some cases. A simple first order backward difference scheme is sufficient if the iterative scheme used to solve the resulting set of equations is implicit, such as Stone's method [45].

Finite difference discretization of the spatial derivatives of energy and species flux is an ideal method to convert the system of coupled non-linear equations into a system of non-linear algebraic equations. A good treatment of the process is given by K. M. Marchand [49]. The non-linear terms can also be linearized through a semi-implicit expression by taking the total change of the term to be the sum of the individual changes in the constituent variables, for example;

$$\mathrm{dF(x,y)} = \frac{\partial \mathrm{F}}{\partial \mathrm{x}}\mathrm{dx} + \frac{\partial \mathrm{F}}{\partial \mathrm{y}}\mathrm{dy} \tag{10}$$

Here, $F(x, y)$ can be replaced with any non-linear term. The method is outlined in detail in [46].

Additionally, the algebraic form Equation (5) acquires, can also be changed by assuming that the total species flux through a single element is constant. This was first introduced by Scharfetter and Gummel [50]. This allows an exact integration of the drift-diffusion equations for a single element of finite length.

3.2 Zero-Dimensional Kinetics

An alternative to the complex spatial solution to the MHD equations is the zero-dimensional kinetics analysis. Here, if the plasma steady state is dominated by volume recombination processes rather than diffusion, as in the case of low voltage application, then the species and electron energy growth can be described by considering total quantities in the NTP. The equations are reduced to the following form [40];

$$\frac{\partial n}{\partial t} = \sum_{i=1}^{k} R_i - \frac{D_a}{\Lambda^2} n \tag{11}$$

$$\frac{\partial E}{\partial t} = \frac{P}{V} + \sum_{i=1}^{k} R_i \Delta E_i \tag{12}$$

$$R_i = n_1 n_2 k_i \tag{13}$$

$$k_i = \int_{Ea}^{\infty} \epsilon Q_i(\epsilon) f(\epsilon) . d\epsilon \tag{14}$$

$$\frac{1}{\Lambda^2} = \left(\frac{\pi}{L_1}\right)^2 + \left(\frac{\pi}{L_2}\right)^2 + \left(\frac{\pi}{L_3}\right)^2 \tag{15}$$

Where, n is the number density, R is the reaction rate term, D_a is the ambipolar diffusion coefficient, Λ is the diffusion length, P is the applied power, V is the reactor volume, E is the mean electron energy is eV, ΔE is the energy gain or loss for the reaction, ϵ is the

electron energy, L is the dimension of the reactor (length, width and height), k is the forward rate constant and E_a is the activation energy, which is equal to ΔE.

Here, R is determined using the solution to the Boltzmann equation. The second term in the species conservation equation, Equation (10), accounts for loss of charged particles due to diffusion towards the walls of the reactor.

In this study BOLSIG+ [34] was used to obtain the rate coefficients at a given energy level. A good approach outlined by R. Aerts [51] is to develop "look-up tables" of energy against rate coefficients for each reaction. In this manner, BOLSIG+ can solve for a range of mean electron energies and provide rate constants using the obtained electron energy distribution function. As an alternative, it is also possible to assume a Maxwellian distribution for the electron energy distribution function but will reduce the accuracy of the results or use the classical Arrhenius form given in Equation (1).

The equations are first order ordinary differential equations, and hence, they can be solved using several numerical approaches. In this study, a first order backward difference was used to discretize the time derivatives for all species and electron energy. To avoid instability arising due to a fully explicit evaluation of the electron energy equation, the semi-implicit linearization method described in [45] is used.

Figure 1, as an example, shows the difference in stability for the following conditions.

Initial electron density of 10^6 m^{-3}, initial mean electron energy 1 eV and 100 Pa pressure and 273 K temperature. 300 V and 1 mA sinusoidal waveform at 13.56×10^6 Hz were assumed for power input to the plasma. Time step size was 3.69 ns.

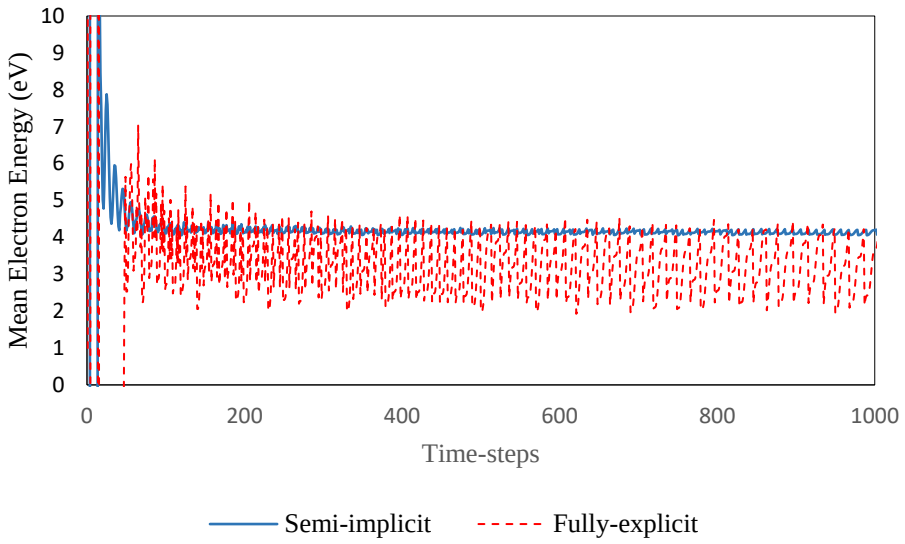

Figure 3. Showing the mean electron energy growth with time for a semi-implicit stable scheme and fully-explicit scheme.

The fluctuations can be minimized by reducing the time-step but considering the total number of reactions and species, the computation time can be enhanced by keeping a larger time-step and implementing a linearization scheme.

Figure 2 shows the characteristic fluctuation in the solution that grows and decays with the power waveform. The time-step was 1/500th of the time-period. As the pressure increases the tendency of the solution to become unstable increases. Since the source terms are larger in magnitude and can easily over or under-predict after an interval of time. If that interval is small, then the prediction is close enough to eventually converge. It can be shown that for the mass conservation equation, the instability will not expand if $n_2 k_i \Delta t > 2$ [48].

Conversely, the semi-implicit scheme although relatively stable, will also display a fluctuating solution if the time step is large. The linearization is not strong if higher derivatives are ignored in the Taylor-series expansion.

3.3 Advantage of Zero-Dimensional Kinetics Modeling

This type of model has some advantages in terms of simplicity and computation time. Since the solution is mainly concerned with the time evolution of the electron energy and species densities over time, there is no restriction on the time-step that arises from spatial discretization (Von-Neuman Stability criterion).

Additionally, various reactor geometries can be simulated but the effect is reproduced only in the volume of the design. The specific geometry affects the characteristic diffusion length and hence diffusion losses of charged and excited species. Note that in the presence of a di-electric barrier, the diffusion losses are suppressed and charge/species conservation is a result of volume recombination processes such as attachment or electron-ion recombination or ion-ion recombination [39].

Various input power waveforms can be studied easily. The most important ones commonly seen in CO_2 dissociation studies are pulsed type and AC waveforms. Care should be taken when applying a high-power signal such as 25-50 W to a small discharge volume. Since, it is assumed that initial electron density will be low, a high power per unit volume ratio will result in initial electron temperatures to acquire unrealistic values but as the solution progresses, the increasing electron density causes a rapid decay of the electron energy towards a realistic solution.

In a DBD reactor, a high voltage signal is provided to generate a large number of electrons in a relatively short time interval. A Zero-D Kinetics model does not require the initial current to be known and if the power waveform is known at steady state, it can be inserted into the model. After a few time-steps, the results converge onto the steady-state solution. In a One-Dimensional model, the electron and species flux has to be known as a function of space and hence cannot be solved without factoring in the evolution of current (electron flux) through the reactor.

In the first few cycles, the electron density is quite low and hence, plasma conductivity is low. The initial discharge current is consequently low. It can be estimated from Equation (16),

$$I = q\mu_e n_e E \tag{16}$$

Where, q is the elementary charge and *E* is the electric field strength. To obtain the value for *E*, the reduced electric field strength (*E*/*N*) can be obtained via BOLSIG+ and converted into E by multiplying with the neutral gas density, *N*.

CHAPTER 4

RESULTS

In this study, the multi fluid approximation is used to examine the effect on dissociation rates of several compounds such as CO_2, Argon, Helium and their mixtures. The effect of varying the applied voltage frequency, pressure, reactor diameter, gas temperature and dielectric thickness and length on the reaction rate and power dissipated in the reactor is examined. The first set of results presented in sections 4.1 to 4.7 correspond to a multi-fluid approximation of a plasma. The fundamental conservation equations of mass, momentum and energy are solved. The results include distributions of number densities of electrons, ions and excited species and the reactions rates.

Focus is kept on the shape of the distribution profile rather than the actual numerical values. First, the spatial distribution for all the species are given, followed by key reaction rates. In section 4.9, the design recommendations based on the profiles is given. Since an optimization analysis is beyond the scope of this study, only qualitative methods are given for some key parameters such as applied voltage.

A quantitative analysis is presented in section 4.8 by the zero-dimensional analysis.

4.1 Multi-Fluid Model (MHD) Validation

A plasma state will dissociate any species within its composition if the conditions are favorable. A molecule within a plasma will dissociate via several possible paths which are different types of collisions. To accurately describe the chemical kinetics involved, all species and their respective collision cross-sections must be considered.

However, for some gases like Helium and Argon, a detailed chemical model is not required to accurately predict the discharge.

In order to conduct a sensitivity analysis on a pure CO_2 model, a validated approach is required to ensure the solution to the fluid equation under the physical conditions can be relied upon. The case adopted here represents a capacitively coupled discharge. This refers to a parallel electrode configuration with or without a dielectric surface. One of the electrodes is grounded while the other is provided an AC or DC voltage or current signal.

First, the results from the one-dimensional fluid simulations are presented in Section 4.2 and the results from the zero-dimensional kinetics are presented in Section 4.8. The comparisons are provided in the relevant sections. Since the purpose and conclusions drawn for each model was different, they are presented separately.

The purpose of validation is to show that the conditions under which a CO_2 sensitivity analysis will be carried out are realistic and that fluid equations can indeed capture a wide range of conditions. Here the simple case of a Helium RF discharge is presented.

Table 1 shows that the results agree with the experimental data in [52]. The results are well within the standard deviation of similar models from various research centers. Additionally, fluid approximations for NTP's do not provide accurate results under low pressures [52].

Figure 4 shows a characteristic noble gas distribution. Similar findings for Helium are given in [52] and for Argon in [43].

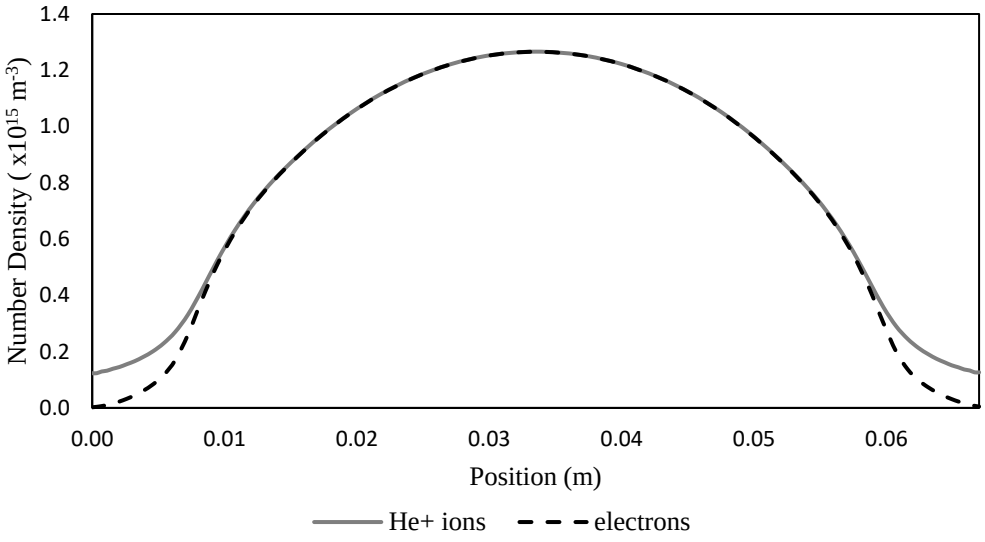

Figure 4. Spatial distribution of He+ ions and electrons in the RF Helium discharge. At an applied voltage of 300 V, AC frequency of 13.56 MHz and gap length of 6.7 cm.

Table 1. Model results for CCP Helium discharge from the one-dimensional fluid simulation.

	Pressure (Pa)	Electron Number density (cm^{-3})	Mean Electron Energy (eV)
Model	4.00	1.37×10^{8}	14.71
	13.33	6.18×10^{8}	7.31
	40.00	1.25×10^{9}	5.48
Experiment [52]	4.00	2.8×10^{8}	9.60
	13.33	12.0×10^{8}	6.20
	40.00	23.0×10^{8}	4.50

The purpose of the one-dimensional modeling is to examine the distribution and extract qualitative conclusions from the solution. The conversion fractions are expected to be low under the given conditions. A high voltage simulation is performed in Section 4.7 where a zero-dimensional kinetics model is used to incorporate the effects of varying input parameters. A special focus on input waveform and carrier gas is presented.

The objective of this study is not to accurately simulate or duplicate any experimental observations but to obtain a better understanding of the dissociation in the reactor by observing the spatial, temporal growth and decay of the various species and reaction rates.

4.2 Carbon dioxide, reactions and species

For CO_2, it has been shown via experiments that microwave discharge plasmas provide the highest energy conversion efficiency [53, 54]. The experimental studies conducted cover a small range of discharge conditions. In fact, the large chemistry of CO_2, CO and O is not properly investigated in the discharge reactor. This is because the full chemistry significantly prevents 2-D and 3-D computational simulations to proceed quickly. Even 1D simulations can be computationally expensive if the mesh used to discretize the problem domain if too 'fine'.

The model for CO_2 dissociation is difficult to develop, as recent studies show [55]. To accurately simulate any experimental conditions a wide variety of chemical species must be considered and the reaction pathways should be extensively covered.

In this section the first set of results for CO_2 correspond to those obtained via a model restricted to known experimental cross-sections. An extensive effort in compiling CO_2 cross-sections was performed by Itikawa [56] in 2002. The cross-sections contain electron impact cross-sections of CO_2.

The interest in CO_2 dissociation has only recently increased, and hence, cross-sections for several collisions are not yet known experimentally.

Table 2 shows the different reactions selected for the reference case study to determine which reactions have a significant impact on electron energy and density. CO_2 dissociation via an electron into CO by electron impact dissociation ionizations and direct electron impact only. Vibrational excitation can lead to dissociation if the population and level of excited vibrational species is significant. [51] reports a total of 25 vibrationally excited states for CO_2 but the cross-sections for the states beyond the first Asymmetric stretching

mode are derived from the Fridman-Macheract model [39]. Here, the inclusion of the lower vibrational levels serves to examine the growth rate of the excited species. If lower level number densities are insignificant, then higher levels will not sustain themselves owing to decreasing lifetime as excitation level increases.

Table 2. A summary of the Reaction kinetics considered in the one-dimensional model based on published cross-section data from [56].

Reaction No.	Reaction and Type of Collision
1	$e + CO_2 \rightarrow 2e + CO_2^+$
	Electron Impact Ionization (Energy loss = 13.80 eV)
2	$e + CO_2 \rightarrow 3e + CO_2^{++}$
	Electron Impact Ionization (Energy loss = 37.40 eV)
3	$e + CO_2 \rightarrow 2e + O^+ + CO$
	Electron Impact Ionization (Energy loss = 19.1 eV)
4	$e + CO_2 \rightarrow 2e + CO^+ + O$
	Electron Impact Ionization (Energy loss = 19.50 eV)
5	$e + CO_2 \rightarrow 2e + C^+ + O_2$
	Electron Impact Ionization (Energy loss = 27.80 eV)
6	$e + CO_2 \rightarrow 3e + O^{++} + CO$
	Electron Impact Ionization (Energy loss = 54.20 eV)
7	$e + CO_2 \rightarrow CO + O^-$
	Electron Attachment Ionization (Energy Loss = 3.30 eV)
8	$e + CO_2 \rightarrow e + CO_2$
	Elastic collision
9	$e + CO_2 \rightarrow e + CO_2e1 \rightarrow e + CO + O(O^1s)$

		Electronic Excitation leading to Dissociation (Energy loss = 12.00 eV)
10	$e + CO_2 \rightarrow e + CO_2(v001)$	Vibrational Excitation via Asymmetric Stretching (Energy loss = 0.291 eV)
11	$e + CO_2 \rightarrow e + CO_2(v100)$	Vibrational Excitation via Symmetric Stretching (Energy loss = 0.167 eV)
12	$e + CO_2 \rightarrow e + CO_2(v010)$	Vibrational Excitation via Bending (Energy loss = 0.083 eV)

Additionally, from Table 2, the reactant chemistry is fixed to pure CO_2 as the inlet gas. However, the product chemistry is restricted to ions and neutral fragments of Oxygen and Carbon monoxide. In literature one can discover cross-sections for both species but for the reference case considered in this section, those reactions leading to the formation of highly excited O_2 and CO species are ignored.

Hence, in Table 2, the selection of these reactions also serves to incorporate all types of collisions, such as elastic, ionization, excitation and sub-types including dissociative ionization, vibrational and electronic excitation.

Table 3 shows the changes made to the input parameters of the Helium discharge model. The current supply to the powered electrode was replaced with a voltage supply with a peak voltage of 300 V at the same frequency of 13.56 Mhz.

Table 3. Modifications to the Helium discharge model.

Parameters	V_{peak}	λ
Value	300	0.01

This was done to examine the current density at the electrodes. If a current supply is used, the current at the electrode is fixed. If the discharge current through the plasma acquires a high value (>>1 A), then the heat transferred to the bulk gas is significant and the gas temperature can rise significantly [57]. Additionally, a large current can result in an arc discharge. Hence, the total current produced is important from an engineering point of view if reactor design is the primary goal. Instead of fixing the value of current, one would like to see how it evolves temporally under different conditions. A voltage signal is also a popular choice in many modeling studies mentioned in Chapter 3.

The second modification is including a secondary electron emission coefficient (λ). This basically accounts for the electrons emitted from a metal surface when heavy ions collide with the surface. The effect is usually insignificant and thus not generally included unless it is required to sustain the discharge.

The species considered for the reference case are presented in Table 2. In its current state, the chemistry of the discharge is lacking. The reference case does not factor in electron impact collisions with CO or O, but a reduced kinetics model can be assumed if low conversion fractions are expected [58] [59].

Reduced electron mobility was obtained via BOLSIG+. Several values of electron mobility were obtained against mean electron energy in CO_2.

4.3 Reference case

Results obtained for the conditions presented in Table 2 and Table 3 are shown below. They are in qualitative agreement with the established physics of discharges. Figure 5 shows the log of the number densities of the positive CO_2 ions and electrons at $t = 1\times10^{-5}\ s$. At this instance the plasma had acquired the pseudo steady state and no further growth in electron population was observed. The powered electrode is located at left and the grounded electrode is on the right at $\theta = 1$.

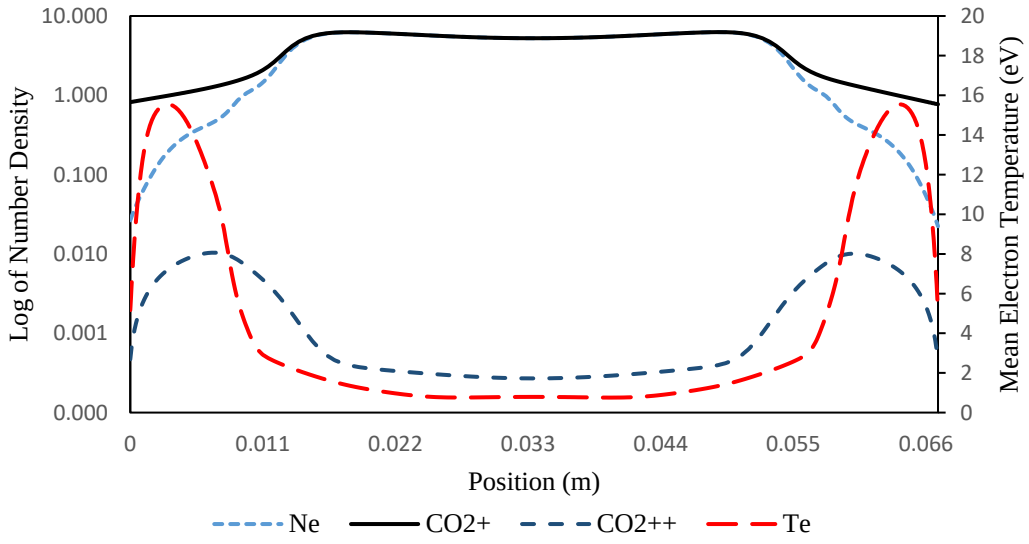

Figure 5. The spatial distribution of the charged CO_2 ions and electrons in the CCP at a time of 10 μs. Applied Voltage of 300 V at a frequency of 13.56 MHz, discharge gap of 6.7 cm.

1. *Species number density distribution*

The spatial distribution depicted in Figure 3 is characteristic of a CCP and non-thermal plasma exposed to a conducting surface [40]. The trend for CO_2^+ and CO_2^{++} ions is an increasing density as distance from the electrodes increases, reaching a maximum close to $\theta = 0.2$. Similarly, for electrons which start off from a negligible density at the electrodes. CO_2^{++} ions show a stronger peak in the sheath and are low in the central region. This distribution can be best explained by examining the reaction set and by the electron temperature distribution. Electron temperature is the highest in the sheath because the electric field strength is strong in the sheath which imparts kinetic energy to the electrons. The low density of electrons in the sheath helps in raising the mean electron energy since a larger portion of the power delivered to the plasma (I-V) is in this region and the energy is distributed to a smaller number of electrons. In this high-energy zone, electron impact reactions with higher threshold energies (Reactions 1 to 6) are activated. As the mean temperature declines towards the bulk neutral region, occupying the major portion of charge species, these processes are suppressed and reactions with low threshold energies have an increased probability for collision. Hence, the flat shape of the He^+ ion

distribution (see Figure 3) observed in the Helium CCP discharge is not seen for CO_2^+ ion. In fact, due to the large number of competitive processes, especially attachment and excitation, collisional probability for ionization is fairly low in the bulk. The probability of collision for a particle moving in a gas of uniform density can be shown to be equal to $\exp(-\frac{z}{\lambda})$ [37], where λ is the mean free path. Since, at any given instant the electron can undergo a number of reactions, the probability of ionization in CO_2 is reduced. Electron attachment is faster than ionization at low temperatures due to its low activation energy. The increase in the probability of collisions, other than ionization, results in a drop-in electron and ion number density. This reduces the ion generation rate in the bulk

The primary ions responsible for maintaining quasi-neutrality are CO_2^+. CO^+, O^+, O^- and CO_2^{++} do not significantly contribute towards the balance of charges. This is mainly due to the lower ionization potential of CO_2. If the applied voltage is increased, it can be deduced based on the cross-sections of the reactions, that CO_2^+ will still be the dominant charged species in a pure CO_2 mixture. In Section 4.7, it is shown that the addition of impurities such as Argon or Xenon in a small fraction shifts the primary positive ion balance from CO_2^+ to Ar^+ or Xe^+. Hence, from a modeling perspective, if accuracy is not the primary goal, higher ionization states of CO_2, CO, O and O_2 etc. can be skipped without significantly affecting the distribution.

CO^+ and O^- ions are not shown in Figure 3 because their densities were comparatively much lower. They are shown separately in Figure 5 and 6.

The low temperatures in the bulk stimulate the growth of vibrationally excited species, which have been of particular interest in recent studies [51]. In this model, only 3 electron impact vibrational excitation modes are included and no relaxation processes for those modes are considered except for a quenching reaction at the reactor walls.

Vibrationally excited states have been proven to be the most energy efficient route towards CO_2 dissociation [6]. The low energy requirements for excitation and relatively high cross-sections enable utilization of low energy electrons. [58] considered 25 vibrational

excitation levels, 21 of which were asymmetric stretching modes leading to dissociation of CO_2 when energy exceeded the C=O bond energy of 5.5 eV [39].

From Figure 6, this fact, of high energy efficiency, is clearly illustrated. The population densities of first vibrationally excited modes are two order of magnitudes above any other species in the model. The peak occurs further from the sheath, and decays towards the bulk. The difference between the maxima and minima of the is larger in the CO_2(v001) excited state. This is largely due to the collision cross-sections over the same energy range.

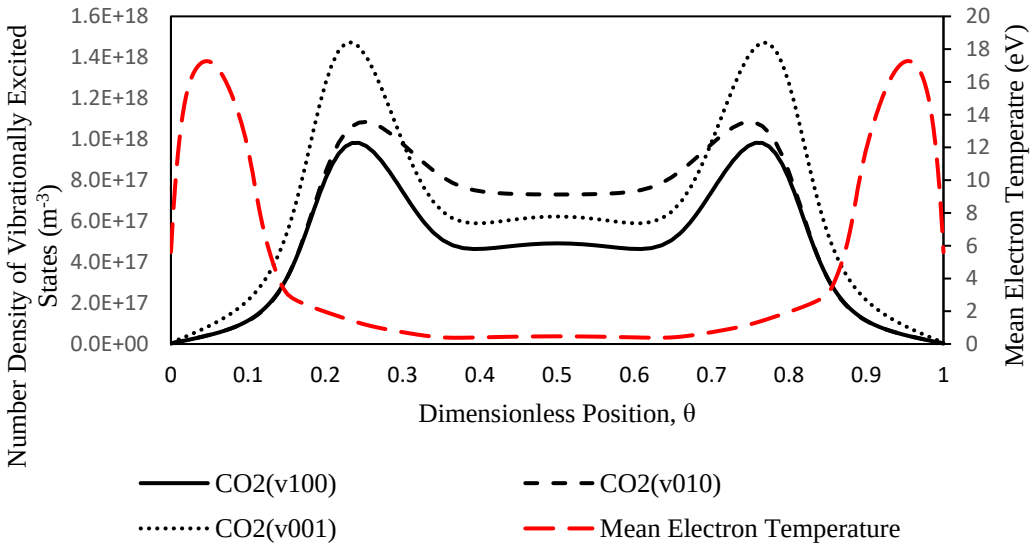

Figure 6. Number densities of CO_2 Vibrationally excited states and Electron temperature distribution in the CCP. Conditions are same as those given in Figure 3.

Vibrationally excited species indefinitely increase as time progresses because of no volume relaxation reactions included in the model. The most important relaxation channels for vibrationally excited CO_2 molecules is Vibrational-Translational (VT) relaxation and Vibrational-Vibrational (VV') relaxation. The former leads to an increase in gas temperature (temperature is defined as the mean translational kinetic energy of a gas particle). The latter accounts for a redistribution of energy within vibrational levels of CO_2 or CO [59]. CO_2 vibrational levels thrive in a microwave discharge but a recent study has shown that the gas temperatures can easily reach 1500 K [59].

From Figure 7, CO is concentrated in both sheath regions and central neutral region. As the electron density increases from the sheath towards the bulk, the number density of CO also increases and begins to drop towards the bulk. The total range however, is between $10^{15} - 10^{16}$ molecules/m^3.

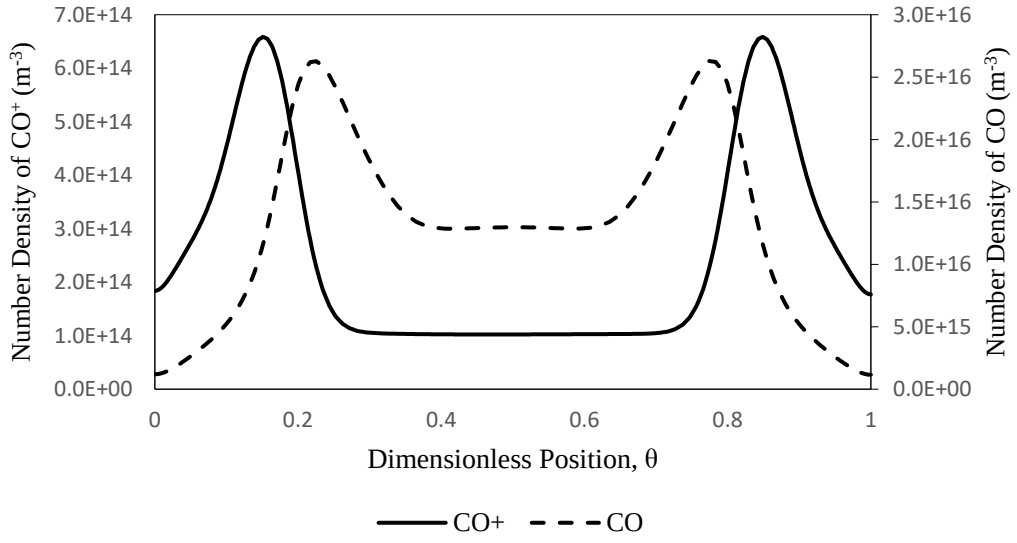

Figure 7. The spatial distribution of the Number Density of CO and CO^+ ions.

Dissociation of CO in this reference case occurs via 3 electron impact ionization reactions (Reaction 3, 4 and 6) and 1 electron attachment reaction (Reaction 7) resulting in an O^- ion. Reaction 8 is an electronic excitation mode leading to dissociation of CO_2. Reaction 4, from Table 2, produces a CO^+ ion.

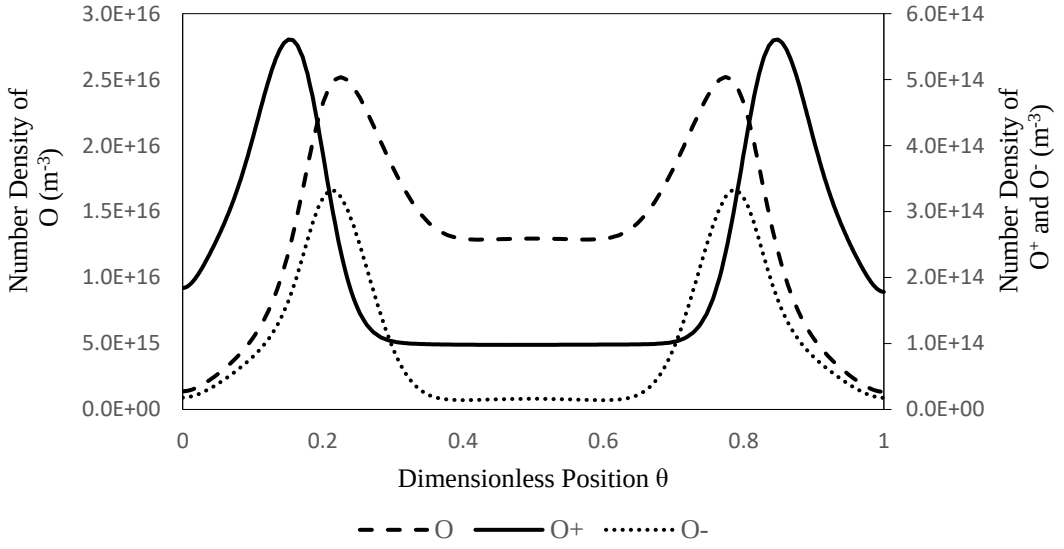

Figure 8. The spatial distribution of the number density of O, O^+ and O^- atoms. The left y-axis corresponds to O atoms and the right y-axis to the O^+ and O^- ions. Conditions are the same as those in Figure 3.

Dissociative Ionization Reactions 3, 4 and 6 require a high activation energy of >19 eV. The regions closer to the sheath provide high energy electrons that contribute to the ionization reactions which are slower in the bulk. In the bulk region, where average electron temperature lies between 1 to 3 eV (see Figure 5) the primary source for CO is due to electron attachment reaction (Reaction 4). The reaction rates are given in Figure 2, which shows a decay of all rates towards the center. However, the electron attachment reaction decays slowly and reaches a minimum close to $\theta = 0.33$. In a CCP, where electrons are lost via diffusion to the walls, the balance of species is not due to bulk recombination processes such as electron ion recombination or ion-ion recombination. Overall electron attachment rates are lower than ionization. If a dielectric barrier is placed on both electrodes, preventing diffusion losses (approximated using the last term in Equation (10)) then attachment reactions will play a significant role in balancing the electron density.

The steady state for CO molecules is not strictly reached because there are no reactions that involve CO on the reactant side.

2. *Reaction rates*

From Figure 7 to Figure 9 we see that time averaged reaction rates (over one RF cycle) and number densities peak close to the sheath region. Figure 9 shows that the time average electron temperature acquires a maximum of 17 eV in steady state. Since Reactions 3 and 4 require high activation energy, it is maximum near the temperature peaks. As the temperature reduces towards the bulk, the rates immediately drop to a very small value. The sheath regions, corresponding to 20% of the total length, have maximum dissociation rates, it means they are largely dominated by the presence of high energy electrons and high electric fields. In the bulk where electrons are high in number but low in temperature, one would expect Reaction 7 to proceed at a faster pace, but attachment dissociation reactions have a very small cross-section, almost 2 order of magnitudes smaller than ionization reactions.

Figure 8 shows the variation of the dissociation reactions along the discharge gap. The rate increase from a small value at the electrodes towards a maximum close to the electron temperature peak. The rate of reaction is a combination of the number of electrons and mean electron temperature.

The cross-section for Reaction 7 is lowest in the energy range 3-4 eV and is zero below it. Reaction 6 is not shown, because of extremely low reaction rates and negligible contribution to CO density. The double peak is due to two factors, firstly the forward rate constant for reactions contributing to CO formation via direct electron interaction peaks twice due to the electron temperature increasing exponentially from the sheath edge and decreasing towards the bulk. The steady state mean electron density increases as shown previously, towards the bulk. Due to the ‘lag’ in two distributions, the product of electron density and the rate constant results in two peaks occurring. For electron attachment, there is a single peak, this is explained in detail below.

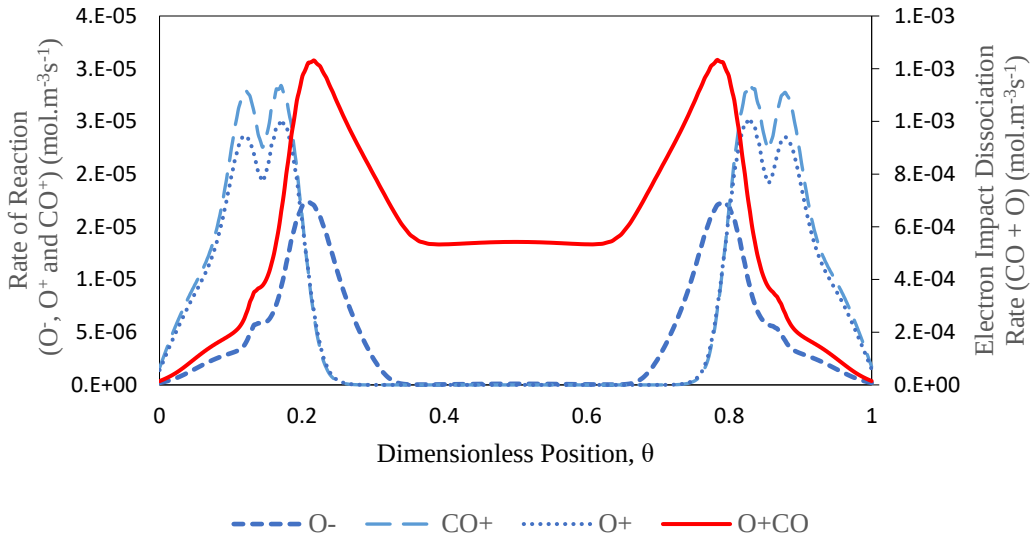

Figure 9. Spatial variation of dissociation reactions rate at 10 μs. Reference case conditions.

1. *Attachment:* The electronegativity of the oxygen atom induces the electron attachment dissociation but at a very slow rate. The cross-section for attachment is low but it is comparable in order of magnitude to the ionization dissociation reactions. This is because a larger fraction of electrons can initialize dissociation via attachment path. Hence, the peaks are towards the electron density peaks and farther away from the temperature peak. Additionally, the peak is not split into two portions as it is for ionization reactions. This is because the dominating factor is electron density which has a smoother trend.

2. *Ionization dissociation:* This requires higher energy as compared to other reactions. The peaks are closer to the temperature peak, implying a stronger dependence on electron temperature, rather than number density. The fraction of electrons occupying higher temperature greater than 19 eV are significantly less compared to the fraction in the bulk which has an average temperature between 1-3 eV. Despite this constraint, the reaction proceeds fast due to higher temperatures in the sheath.

3. *Electronic excitation:* Direct electron impact dissociation proceeds via the production of an intermediate electronically excited state which can be attractive or repulsive. From Figure 7, this distribution displays a strong dependence on both electron temperature and number density. Hence, the peaks are closer to the maximum points in the electron density distribution and rate of reaction at all points is quite high.

The conversion of CO_2 at 300 V is naturally quite low. At a short interval of 10 μs and because of the absence of a di-electric covering on the electrodes, the electron densities are also not high. Table 4 shows the conversion at 10 μs in the reactor using Equations (13) and (14),

$$\eta = \frac{CO_{2,initial} - CO_{2,final}}{CO_{2,initial}} \tag{17}$$

$$\chi = \frac{X}{CO_{2,initial}} \tag{18}$$

Where, η is the percentage change in CO_2 density and χ is the percentage of any product X in the mixture at 10 μs.

Table 4. Conversion fraction of CO_2 and fractions of CO, O and vibrationally excited states of CO_2 in the final mixture at 10 μs. For applied voltage of 300 V, discharge gap of 6.7 cm and frequency of 13.56MHz.

CO_2	4.12×10^{-3}	Total percentage of CO_2 molecules dissociated
CO (CO and CO^+)	5.20×10^{-5}	Total percentage of CO species in the mixture
O (O^+, O^- and O)	5.20×10^{-5}	The amount is equal to CO because the same reactions produce both species.
CO_2 Vibrationally excited states	3.56×10^{-3}	Sum of all three vibrational modes.

The fractions are low but the vibrational states are 2 orders of magnitudes higher than CO and O. This is to be expected based on a low threshold energy. At higher voltages and power input the conversion will undoubtedly increase but for the purposes of this study, the distributions are examined at a low voltage.

To obtain the distribution of the rate of reactions involving CO and O on the reactant side, it is easier to use the obtained temperature distribution and rate coefficients from BOLSIG+. Since, the interest is to see the distribution of the rate of reaction, a 'snap-shot' can be obtained at 10 μs using the known densities from Equation 10. It is understood that the reaction rates will change if the products from the electron impact reactions of CO and O are used. Figure 9 shows the spatial distribution of the reaction rates at 10 μs. The procedure is outlined above.

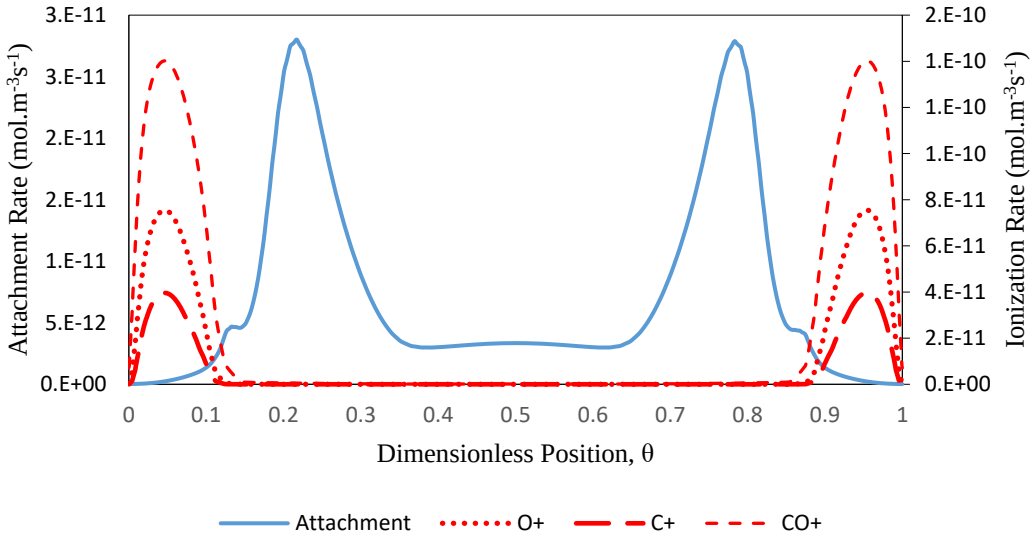

Figure 10. Spatial variation of the electron impact reactions of CO at 10 μs. The left y-axis shows the electron attachment rate and the right y-axis shows the ionization and dissociative ionization rates. Discharge conditions are the same as in the Reference Case.

From Figure 9, the distributions show the same twin-peak distribution as CO_2. The ionization collision rates are dictated largely by temperature and are very much close to the temperature peaks. Additionally, they are suppressed in the bulk and decline rapidly

as the electric field strength decays towards the bulk neutral region. The attachment reaction is favored by a higher electron population and the peak shifts towards the bulk.

The above reference case serves as a basis to further our understanding of the chemical reactions occurring in the CCP under a fixed set of conditions. To better understand the kinetics and output, the sensitivity of the solution to the underlying assumptions has to be examined. At the present state, only a reduced set of electron impact reactions are included and no neutral or ion interactions are considered to reduce computation time and simplify the analysis. Figures 3 to 9 indicate that the relative weights of each reaction will remain independent of scaling-up or down of the reactor.

The spatial distribution curve of CO is independent of the choice of reactor, whether DBD or CCP. In a fluid simulation performed by [60] considering several reactions, the twin-peak distribution is consistent with every reaction path that contributes to the production of CO. The experiment was conducted in a DBD reactor operating in the filamentary discharge regime due to the low applied frequencies. Additionally, the applied voltage in the case of a DBD reactor is usually in the order of kilo-Volts and seemed to have no impact on the relative proportions of reaction rates which produce CO, meaning the shapes are consistent.

4.4 Electron Impact Dissociation Cross-sections of CO_2

In section 4.3, a reference case was established and distribution for number densities, reaction rates and temperature was obtained. In current literature, there are in fact two different sets of cross-sections for electron impact dissociation of CO_2 via electronic excitation. In this section, the sensitivity of the distribution to the choice of cross-section is examined. At first, reactions with available cross-sections are incorporated with the reference of the source provided.

Cross-section is a collision parameter which is strongly influenced based on the reaction type. They are critical in electron impact reactions since the energy of the incoming

electron plays a crucial role. For ion-ion or ion-neutral or neutral-neutral collisions, the variation in energy is limited, since the fundamental assumption of constant bulk gas temperature holds. If the plasma residence time is not too large (greater than 1 s), the gas temperature is not expected to rise significantly.

The set of gas molecules are limited to CO_2 on the reactant side and CO_2, CO and O on the product side. Dissociative Ionization Reactions 5 and 14 are not included because of a very low C^+ and C^{++} number density in the results and an unfavorable increase in computation time. Since these species are not governing the discharge behavior and their removal resulted in negligible change. Under the same set of physical conditions, the gas chemistry is increased to incorporate additional species.

Direct Electron Impact Cross-sections:

Table 1 shows the additional reactions to the set in Table 2. This includes two of the electronic excited states of CO_2. Notice that the electronic excitation state in Table 1 is replaced with Reaction 9*. This is to preserve consistency, since cross-sections for both excited states are obtained from [61]. Finally, Reaction 5 and Reaction 14 include direct electron impact ionization reactions of CO_2 to C. The complete set is consistent with published cross-sections.

Table 5. Reactions added to those in Table 2.

Reaction 9* (Energy Loss = 7 eV)	$e + CO_2 \rightarrow e + CO_2e1$ (Source: [61])
Reaction 5 (Energy Loss = 27.8 eV)	$e + CO_2 \rightarrow 2e + C^+ + O_2$
Reaction 13 (Energy Loss = 10.5 eV)	$e + CO_2 \rightarrow e + CO_2e2$ (Source: [61])
Reaction 14 (Energy Loss = 54 eV)	$e + CO_2 \rightarrow 3e + C^{++} + O_2$

In the reference case, the activation energy of electron impact dissociation reactions and ionization of CO_2 was not lowered. Dissociation will occur more easily if the electron

collides with a vibrationally excited molecule and ionization will occur at a reduced ionization potential if an electron collides with an electronically excited state, since the valence electron has migrated to a higher energy orbital. These two cases are handled by reducing the activation energy by the excited state energy level [51].

The different sources for electronic excitation of CO_2 pose a risk of over estimating dissociation rates. In [61] the excitation potential is lower and will obviously result in higher CO population. The sensitivity of the spatial distribution is given in Figure 10.

Due to the increase in computation time, the solution was not allowed to progress to a pseudo-steady state but instead the various number densities, reaction rates and electron temperatures are examined at 50 and 500 voltage cycles (3.68 μs and 36.8 μs). The different cycle lengths will also provide results that show variation with increasing residence time. Although it is well known that as residence time increases, dissociation rates increase. The shape of the spatial distribution of the number densities still needs to evaluated to see if there is any significant change.

To differentiate the results, the results are split into two cases (one incorporating cross-sections from the Phelp's database and the other involving reduction of activation energy due to excited molecules).

- The first will be referred to as case two (Case II, where direct electron impact cross-sections from the Phelp's data base are considered along with reactions presented in Table 2.

- The second case (Case III), will use the Phelp's cross-sections and the activation energy is lowered by the energy level of the excited electronic or molecular state.

Figure 11 shows the difference between electronically excited states of CO_2. The main difference between the two cases lies in the cross-section and activation energies of those states from the different sources. There is no agreed upon consensus regarding the electronically excited states of CO_2 [56]. In the reference case, all cross-sections from [56]

are considered, while [61] provides different values and 2 different states. The results are different and affect, in particular, the electron population. In the reference case, number densities are low because the activation energy is high (12 eV) and cross-sections are lower in the same energy range. In Case II, the excited state at (10.5 eV) has higher cross-sections. This results in electrons losing more energy in excitation reactions in Case II resulting in a higher number density of CO_2e1 states and lower electron density. The electron temperature is reduced near the sheaths but is slightly higher in the bulk.

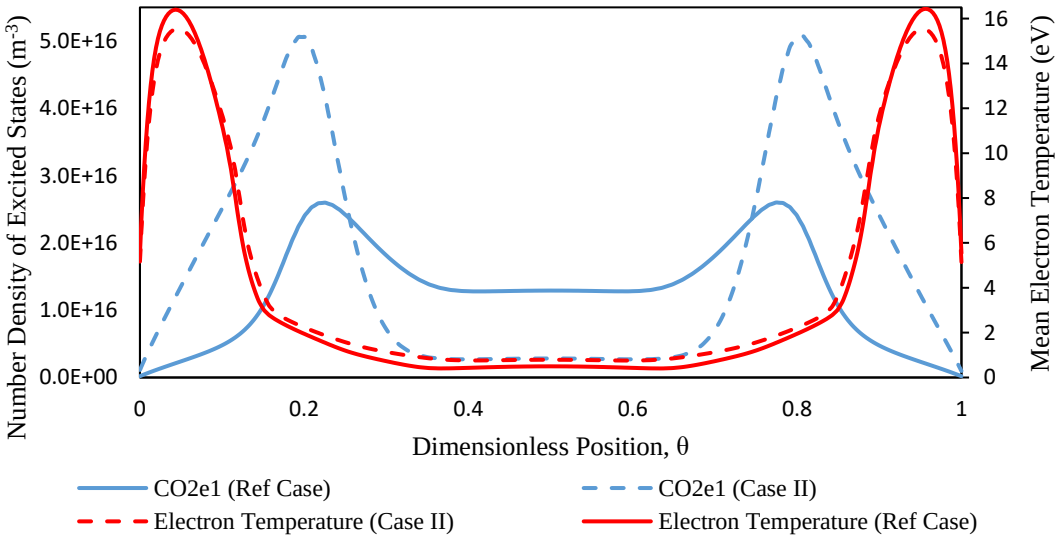

Figure 11. Spatial variation of the Number Densities of the two electronically excited states [61] and electron temperatures obtained from the two Cases. Discharge conditions are the same as in the reference case.

Results obtained from the cross-sections in Table 5 show a significant quantitative difference in the number densities of the excited states. CO_2^{++}, C^+ and C^{++}states were found to be negligible in the applied conditions and were eliminated. It is noted that by including positive ions of C and higher ionic states of CO_2 the simulation time drastically increases.

The selection of the relevant cross-sections of the electronically excited states has a significant impact on the electron number densities. It ties strongly to the results obtained.

Since, electron growth rates, number density and mean energy influence every electron impact reaction, using different cross-sections can significantly offset results.

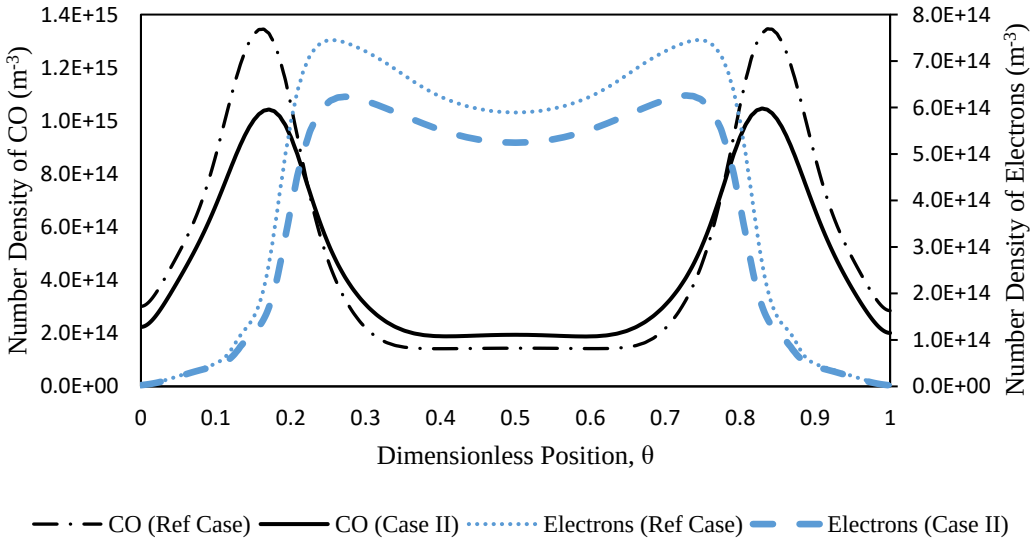

Figure 12. Spatial variation of Electron and CO density for the Reference Case and Case II.

Figure 12 shows that as electron density reduces (see above) so too does the CO density. If the discharge model consists solely of electron impact reactions, then one can expect such a situation. A key point to note is that the form of the distribution, mainly the trend is undisturbed by the choice of the cross-section. There is a shift in magnitude which is expected by the lower threshold energies. The shift is primarily in magnitude and does not disturb the profile. Hence, the profile depends mainly on the ionization potential of CO_2 for the production of electrons and energy consuming excitation reactions.

Figure 12 shows a comparison between the reduced electric field strength, reduced electron mobility and reduced electron diffusion coefficient for the two cross-section sets.

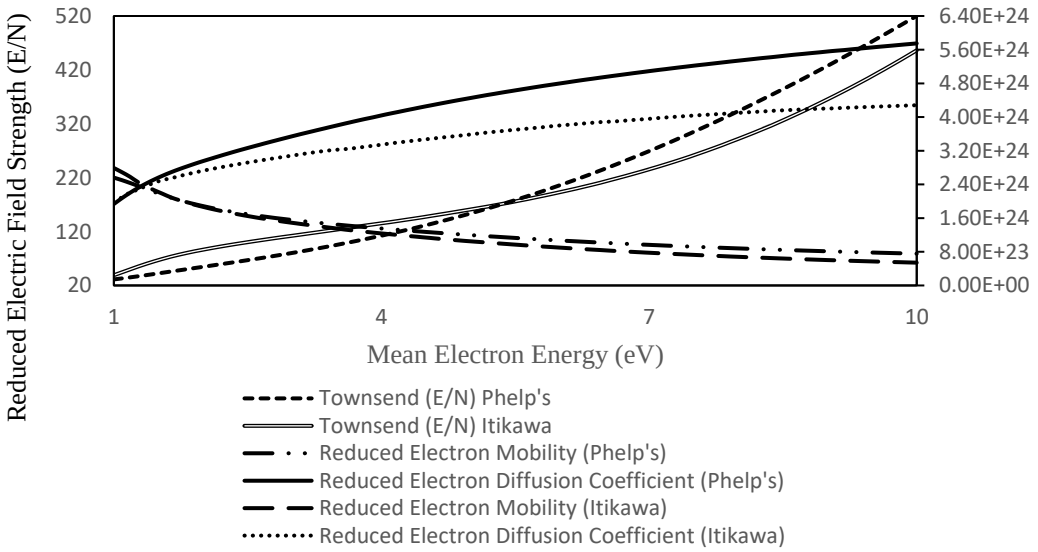

Figure 13. Comparison of electron transport properties and reduced electric field strength in a CO_2 plasma based on two different cross-section sets.

The difference tends to enlarge towards increasing mean electron energies, which is understandable since probability of formation of an electronically excited state is higher based on the cross-sections from the Phelp's dataset. Electron mobility is reduced if electron to neutral collision frequency is high, which is the case if only a single excited state is considered. Hence, transport properties for electrons are lower in the case for Itikawa's dataset because of an increased electron-neutral collision frequency.

4.5 Effects of Activation Energy Reduction and Effects of Residence Time

The results presented in Section 4.1 include all electron impact collision reactions using published cross-section data. Now we consider the effect of electron collisions with electronically and vibrationally excited molecules. The method is outlined in Section 4.4.

The ionization potentials for Reactions 1 and 2 were reduced by the energy level of the electronically excited states CO_2e1 and CO_2e2. Reactions 3, 4 and 7 were treated in the same manner considering the 3 vibrationally excited states. Higher vibrational states are not considered.

Table 6 shows the total number density of the 3 different cases. Case III has higher densities when compared with Case II. This is due to the increase in ionization rates of CO_2 because of the presence of excited states. This goes to show that considering the excited states can be crucial towards accurate modeling. Since higher vibrational states do not typically thrive in a CCP or DBD, they were not included but lower quantum levels can also contribute towards dissociation in a significant manner. Additionally, the voltage in all cases was kept low at 300 V. At higher reduced electric field strengths, vibrational modes are suppressed and ionization reactions are dominant.

Table 6. Showing a comparison between Case II, Case III and the Reference Case.

Time	Scenario	CO_2^+ (10^{13})	CO (10^{13})	e (10^{13})
50 RF cycles	Case II	2.41	0.959	2.20
	Case III	2.45	0.967	2.24
	Reference Case	2.97	1.13	2.75
500 RF cycles	Case II	2.69	3.11	2.48
	Case III	2.74	3.15	2.53
	Reference Case	3.19	3.41	2.96

In this analysis, the reactions involving the product ions and neutrals were not included. In such a case, the residence time should be kept short in order to avoid drastic errors arising from a simplified model. The total simulation time was 36.9 μs whereas residence times can exceed 1 s depending on the flow rate.

From the above analysis, it can be concluded that for short residence times, the choice of electronically excited state has a significant effect on results. CO_2^{++} and other ions do not contribute significantly towards quasi-neutrality and generally do not affect dissociation rates. Vibrational states have an impact in increasing electron production via stepwise ionization. They are also crucial towards the electron energy balance. If these reactions are ignored, then the model has to be compensated by accounting for the additional energy losses.

4.6 Effect of Applied Voltage and Pressure

The reference case gas chemistry was subjected to a sinusoidal voltage waveform with a peak voltage of 300 V. Experimental observations from numerous sources verify that an increased voltage results in an increased mean electron energy and number density. The increase in applied voltage results in charged particles (ions and electrons) acquiring a higher velocity. The work done by an electric field depends on the magnitude of the charge only. Owing to the extremely small charge to mass ratio of electrons, they are accelerated to higher velocities. Thus, the fraction of electrons occupying a higher energy range increases since they exchange of kinetic energy between electrons and molecules is not significant. However, ions undergo collisions with the bulk gas and essentially remain at the same temperature as the background gas but this is not the case if excitation reactions are dominant and persist for higher residence times. Ions collide with neutral gas molecules/atoms and exchange the energy efficiently which results in negligible increase in the mean ion energy.

As is expected of any plasma state, an increase in voltage corresponding to an increase in energy supplied to the plasma electrons resulted in a larger electron population growth rate as well.

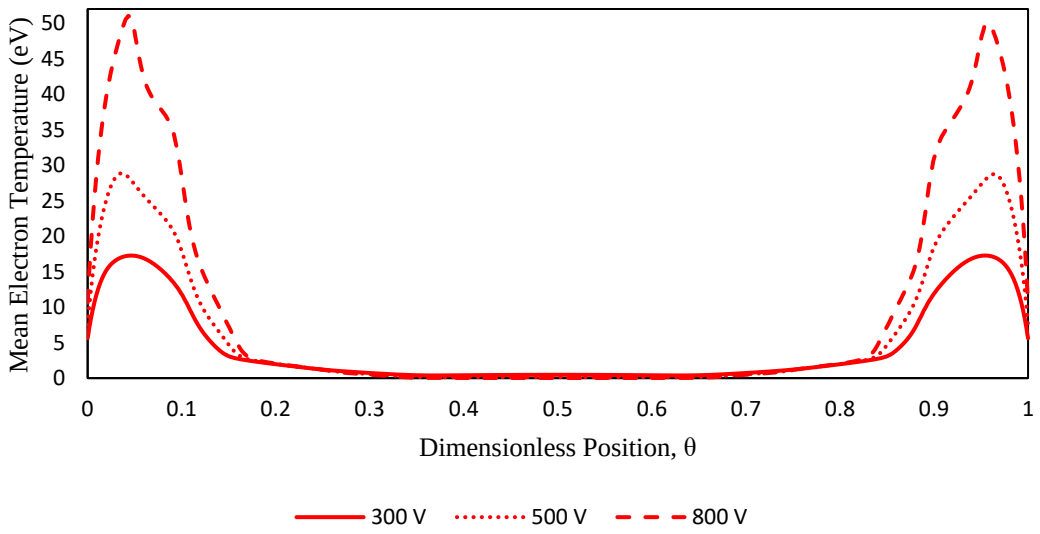

Figure 14. Electron Temperature distribution in the CCP at t = 36.6 μs.

The electric field strength is increased as voltage is increased, resulting in higher temperatures in the sheath regions as shown in Figure 14. The bulk region, is still at the same average temperature range regardless of the applied potential. This is expected, since the sheath shields the bulk plasma from the external electric field. The electrons in the bulk do not gain sufficient directed kinetic energy in the presence of a weak electric field. It is small enough to sustain a discharge current. The sheath length also increases, due to increasing electron number density.

The total time averaged number density spatial distribution is shown in Figure 15.

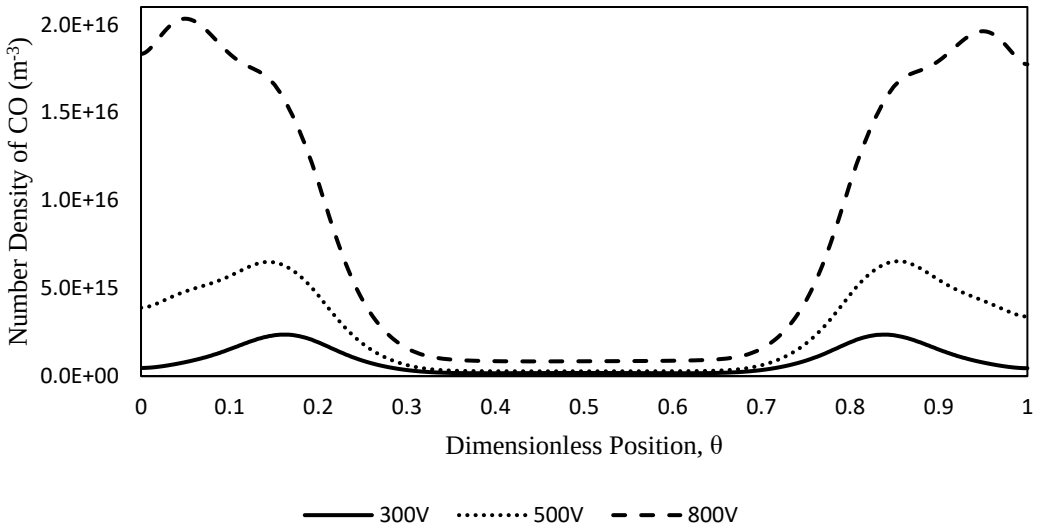

Figure 15. Total CO molecule time averaged (over one RF cycle) number density distribution in the CCP at t = 36.6 μs.

The difference between the time average from one RF period did not differ from the instantaneous distribution because unlike charge particles, neutral molecules like CO diffuse purely by a difference in concentration gradient. So, the peaks correspond to regions where electron temperature is highest. Since, Reactions 3 and 4 are electron impact ionization dissociation reactions, a larger contribution is observed as opposed to Reactions 6 and 7 to the overall production rate of CO.

Hence, the applied potential strongly affects the dissociation rates and electron production in a CCP. Its effect is quantified in most studies as specific energy input to the plasma. It is defined as the ratio of the discharge power to the input flow rate. The discharge power however, changes with time. If the maximum input power is taken and the flow rate computed by dividing the reactor volume by residence time (in this case it is 10 μs from the reference case), the SEI from Equations (15) and (16) for 300 V is obtained,

$$SEI = \frac{P}{Q} \tag{19}$$

where Q, the input flow rate is given as,

$$Q = \frac{V}{\tau} \tag{20}$$

The electrode area was assumed to be 1 m^2. This is unrealistic but is consistent with the helium model. The volume is 0.067 m^3. SEI is then 522 J/cm^3, which is a very high value. However, based on the spatial profiles, the bulk of this energy is transferred to the sheaths, reflected by the high electron temperatures. Since, the work done on a charge by an electric field (between collisions) is given as, $W = \int_{x1}^{x2} Eq.dx = \frac{1}{2}mv^2$, more kinetic energy is gained by electrons in regions where electric field strength is high.

Combining Equations (15) and (16), it can be seen that SEI is directly proportional to residence time, hence the longer the residence time, the more energy is given per molecule. However, residence time can be influenced by changing reactor volume or adjusting the flow rate. A larger residence time positively influences dissociation but an increase in reactor volume lowers the power density and dissociation can start to decline. An optimal point depends strictly on the design of the reactor and input conditions.

The pressure in all the results was kept fixed at 300 mTorr. At low pressures (close to vacuum), elastic collision rates and electron energy losses in those collisions are low. If the pressure is increased, the elastic scattering probability increases and electrons lose their energy in such collisions which result in low number densities.

From a design point of view, the results from sections 4.1 and 4.6 indicate that a higher voltage setting is desired for dissociation of CO_2. A low voltage of 300 V does not initiate significant dissociation and conversion is low. Increasing the voltage will provide greater dissociation but external resistances need to be included to avoid large current through the plasma. Higher flow rates mean lower residence time and decreasing conversion of CO_2. Hence, if the objective is simply to maximize conversion, a high voltage in the range of several kilo-volts is recommended and is typical of any DBD discharge.

Electrode gap length should be kept low compared to the length of the reactor. It is seen that direct electron impact reactions are higher close to the sheath, hence increasing the

gap length will further reduce the electric field and decrease mean electron temperatures. A longer reactor will enable higher flow rates while not losing the advantage of a strong local electric field. A cylindrical geometry with an inner electrode (grounded or powered), and an outer electrode will be a desirable choice. It is also to be noted that lower voltage (few kilo-volts) but smaller gaps (MHCD reactors), will increase electric field strength and not consume too much power.

4.7 Effect of Argon and Xenon mixtures

The pure CO_2 plasma gains electrons primarily through the ionization of the CO_2 molecules into CO_2^+ as shown in Reaction 1, Table 2. If a gas is introduced which has an ionization potential close to that of CO_2 and recombines with electrons at a slower rate compared to the other reactions, then it can potentially raise the electron number density in the mixture. Argon is one potential candidate. In this section the effect of adding Argon, Helium and Xenon into the mixture on the spatial distribution of species and ionization rate is investigated.

An area that is not thoroughly examined in CO_2 discharges is the addition of a gas that can help raise the growth of electrons in the mixture and does not react to the radicals or species that form in the mixture thus ensuring the overall kinetics stay intact. O. Taylan [62] experimentally investigated the addition of Argon in the CO_2 mixture in an MHCD. This resulted in higher dissociation and was attributed correctly to the increased number density of electrons. The model presented in this study accounts for all electron impact reactions with CO_2 molecule and because the applied voltage is low, conversion percentage is also low. This simply allows a simpler model without having to incorporate CO, O or C chemistry. If the conversion of the products was higher, as in the case of DBD discharge studies then this model will undoubtedly not provide good results.

When impurities are added to a pure gas, the discharge behavior can dramatically change. This is true for many high-pressure discharges, for example in [63, 64], the role of trace impurities of Nitrogen is modeled for an atmospheric glow discharge in Helium in a CCP

reactor. The strong dependence of the number density profiles on trace impurities was shown.

Although an impurity in a CO_2 mixture, the addition of Argon in small quantities provides several advantages. Firstly, it is a Noble gas and does not easily form stable compounds with other molecules. The chemical kinetics of Argon is well established. Table 7 shows the basic reactions of three noble gases, Xenon, Helium and Argon [65],

Table 7. Basic Argon, Helium and Xenon electron impact reactions and threshold energy.

	Reaction	Type	ΔE
1	$e + Xe \rightarrow 2e + Xe^+$	Ionization	12.13 eV
2	$e + Xe \rightarrow e + Xe^*$	Excitation	8.315 eV
3	$e + Xe \rightarrow e + Xe$	Elastic collision	-
4	$e + He \rightarrow 2e + He^+$	Ionization	24.6 eV
5	$e + He \rightarrow e + He^*$	Excitation	19.82 eV
6	$e + He \rightarrow e + He$	Elastic collision	-
7	$e + Ar \rightarrow 2e + Ar^+$	Ionization	15.7 eV
8	$e + Ar \rightarrow e + Ar^*$	Excitation	11.55 eV
9	$e + Ar \rightarrow e + Ar$	Elastic collision	-

Upon ionization, a free electron is available and is not easily recombined with Ar^+. This results in a net increase of available electrons. The ionization potential is higher than that of CO_2 and the excitation potential is also high. However, like Argon, Helium and Xenon also provide free electrons. In this section the increase in electron population for different concentrations is shown and explained by examining the cross-sections and chemical properties of the gases.

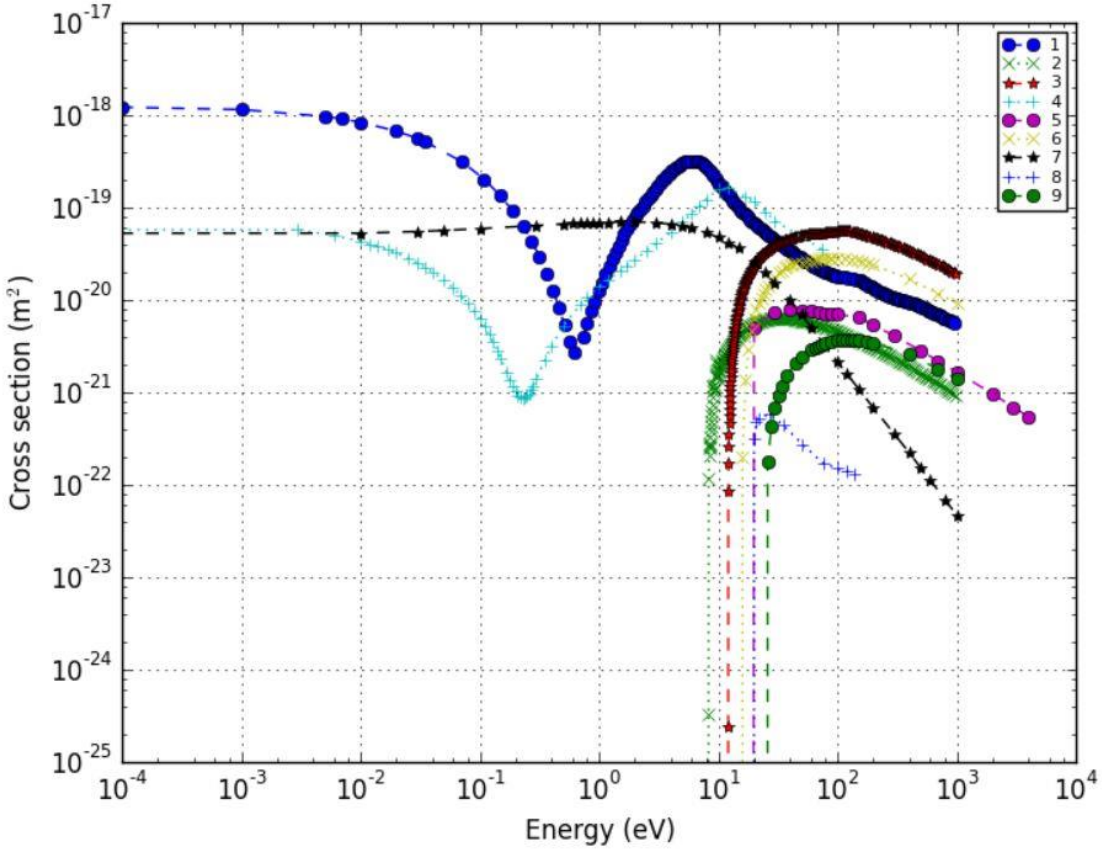

Figure 16. Cross-sections for reactions listed in Table 6 for Xenon (1-3), Helium (4-6) and Argon (7-9) against electron energy (eV) [65].

The mean electron energy of the electrons under the conditions of 300 V and 300 mTorr pressure in the CO_2 model considered in Case III is at a maximum 9 eV and minimum of 3 eV in steady state. The cross-sections for the 9 reactions are shown in Figure 9. As the energy increases elastic collision reactions (1, 4, 7) start to decline primarily because the energy exchange between a high-speed electron and heavy atom becomes more unlikely as the velocity of the smaller mass increases (electrons). Ionization reactions (3, 6, 9) also start to decline in the energy range of 10 to 1000 eV. Such energy ranges are encountered only in high voltage applications.

From Figure 13 it is obvious that the reaction rate for Xe is much higher and will yield more free electrons in a CO_2 mixture. The spatial distribution changes its shape by

flattening in the low energy quasi-neutral region. In this region, compared to Ar, Xe can provide more free electrons since the ionization potential for Xe is closer to collisional processes in CO_2. Hence, a larger fraction of electrons can initiate ionization in Xe. For Argon, the ionization potential is higher than CO_2 hence it is unable to affect the shape of the distribution but still yields a higher electron density. Electron temperature declines slightly in the case of Xe because the excitation potential is lower, increasing the electron energy loss rate due to excitation.

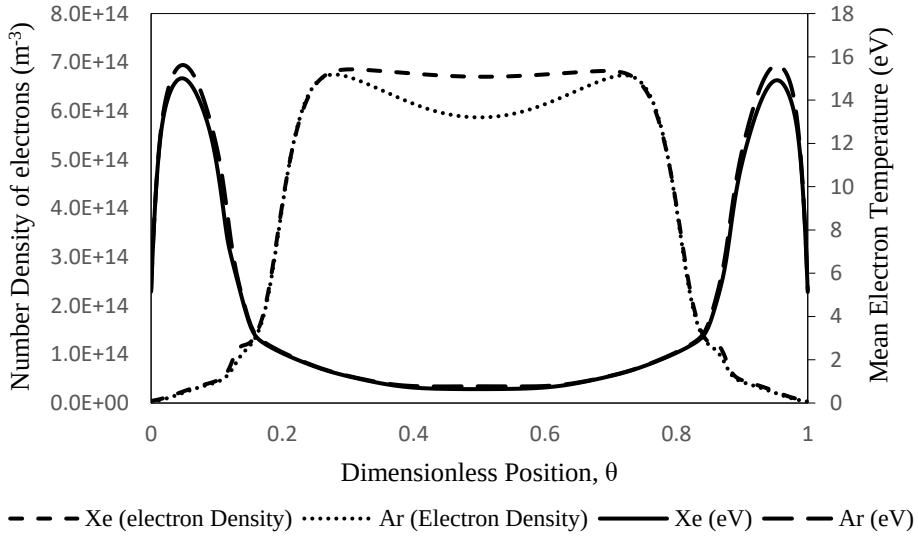

Figure 17. The spatial distribution of electron number density and mean electron temperature in CO_2/Ar and CO_2/Xe mixtures. Initial CO_2 mole fraction was 0.85.

Additionally, the electron-ion recombination rates are quite low in the case of Xenon, Argon and Helium. As outlined in Chapter 2, in atomic gases, dissociative recombination is the mechanism for recombination losses for electrons. It proceeds, first, via the production of a dimer ion e.g. Xe_2^+ and then an electron impact dissociates the ion into the neutral state. Table 8 shows the dimer ion formation rates at room temperature and corresponding dissociation rates at 1 eV. As the temperature of ions and electrons increases, this dissociation rate decreases [40].

Table 8. Recombination pathways and rates for Xenon and Argon at 1 eV.

Reaction	Rate constant
$Xe^+ + Xe + Xe \rightarrow Xe_2^+ + Xe$	$4\times10^{-31}\ cm^6s^{-1}$
$e + Xe_2^+ \rightarrow 2Xe$	$2\times10^{-7}\ \ cm^3s^{-1}$
$Ar^+ + Ar + Ar \rightarrow Ar_2^+ + Ar$	$3\times10^{-31}\ cm^6s^{-1}$
$e + Ar_2^+ \rightarrow 2Ar$	$1\times10^{-7}\ \ cm^3s^{-1}$

Xenon recombines at a faster rate as opposed to Argon. The Xe^+ density at 3.68 μs was higher than CO_2^+ ion density, 6.26×10^{13} and 2.74×10^{13} respectively. The ionization rate constant obtained from BOLSIG+ for the reaction set given in Case III is $1.66\times10^{-15}\ m^3s^{-1}$. From Table 8, the reactions rates can be assumed for a gas density of $9.45\times10^{20}\ m^{-3}$ and a Xe mole fraction of 0.05. The rate of ionization is $6.03\times10^{16}\ m^{-3}s^{-1}$ while recombination rate is $5.12\times10^{10}\ m^{-3}s^{-1}$.

At a Xenon mole fraction of 0.15 the mean electron energy fluctuates between about 5 and 8 eV. The rate coefficients for Ionization at those energies are $3.8\times10^{-15}m^3s^{-1}$ and $2.95\times10^{-16}m^3s^{-1}$ respectively. Since, the rate of recombination decreases with increasing electron energy, an upper estimate for the rate of reaction can be obtained from Table 7. The rate of ionization and formation of Xe_2^+ corresponding to 8 eV are $1.38\times10^{19}\ m^{-3}s^{-1}$ and $5.12\times10^{17}\ m^{-3}s^{-1}$ respectively. The difference is nearly two orders of magnitude. Hence, with an increasing fraction, the recombination is higher due to the increased number density of Xe atoms. Calculations need not be repeated for Argon as it recombines at a lower rate.

The total ionization rate contribution, in other words the total electron production rate is shown in Figure 15 for both Xe and Ar fractions of 0.15.

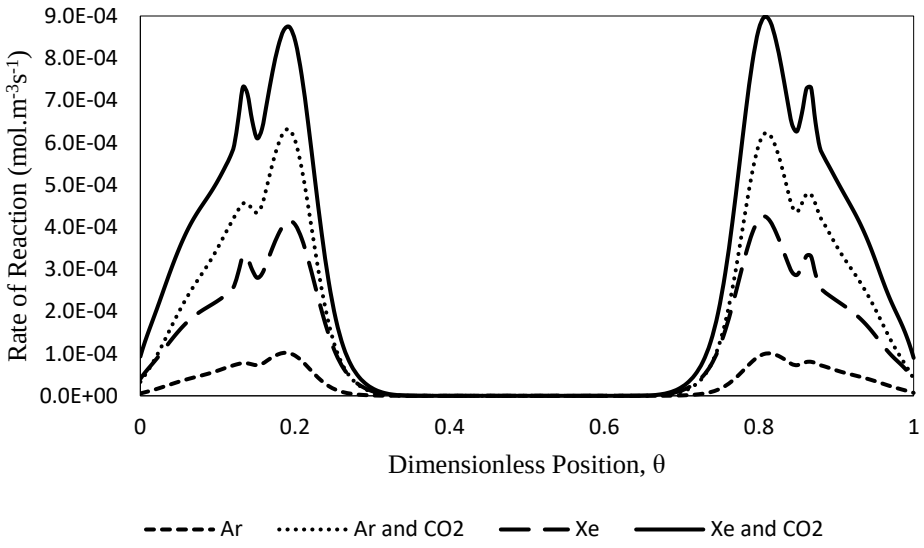

Figure 18. Spatial distribution of ionization rates for Ar and Xe. Total electron production rates including CO_2 ionization are also shown. Discharge conditions are the same as the Reference Case.

In both cases the electron production rate is significantly enhanced. This effect will be increased under high voltages. As explained previously, pure Ar gives a small contribution but its injection results in an increased CO_2 ionization rate. Therefore, the total rate is significantly higher at each point. M. Ramakers [66] experimentally investigated the electrical characteristics of CO_2 dissociation in Ar or He mixtures. They concluded based on their DBD design that Ar or He addition enhances the electron impact dissociation reaction of CO_2. The rate constants were higher at a given mean energy level.

From an engineering stand point, Ar would be the optimal choice. The cost of Ar is much lower than Xe and it results in a noticeable increase in electron production, even at low voltages of 300 V and mole fractions of 0.15.

In conclusion, the addition of these noble gases increases the overall electron density. The spatial distribution is also affected, in the case of Xe, the bulk contains more electrons and tends towards the flat, bell shaped curve commonly seen in pure noble gas discharges. This results in increased ionization of CO_2 leading to the formation of CO_2^+.

The recombination rates for noble gases are extremely low, which indicates that electrons will not be lost via this path for low concentrations. However, increasing concentrations can cause the noble gases to drain significant applied power. From Figure 18, the of the fraction of power dissipated in ionization of CO_2, on 55% (averaged over the reactor), is consumed by CO_2. Addition of Argon and Xenon can have negative effects on conversion efficiency. This also depends on the design, but the criteria for selection of Argon or Xenon fractions should be a power consumption of less than 50 %. Hence, maximum mole fractions of 0.15 are recommended as a starting point.

4.8 Design Recommendations

The results thus far can enable better designing of a NTP reactor dedicated for CO_2 dissociation.

- Firstly, from Figure 14, the increase in voltage resulted in a higher sheath temperature which leads to a higher dissociation rate. The bulk temperature did not increase indicating that the activity remains largely with the sheath. An upper limit to applied voltage can be achieved if energy efficiency is considered. It was not examined in detail in this thesis but generally as applied voltage increases, conversion efficiency declines [62]. This is a compromise, and further investigation into efficiency is required to arrive at an optimal voltage value. However, strictly speaking, conversion fractions will increase as applied voltage increases.

- From Figure 5 to Figure 10, the sheath region contributes primarily to the breakdown of CO_2. Formation rates of CO via dissociative ionization, electron impact dissociation ionization and attachment are high close to the sheaths and in the sheaths but are fairly suppressed in the bulk. It is advantageous to have a larger sheath region. This can be achieved by a CCP design, since the electron number density is less in these reactors, the sheath will enlarge. Additionally, in a DBD reactor the dielectric thickness can be lessened to incorporate the same effect but

since they are not dominated by diffusion, the number density of electrons is higher and sheath temperature decline comparatively.

- The discharge gap should be kept in the millimeter range to ensure high electric field strength. In an MHCD, the gap is typically in micrometers which leads to the discharge phenomenon being slightly different. If the frequency is low, the discharge is filamentary, with current pulses non-uniformly distributed over the surface of a dielectric. A high frequency, typically radio-frequency of 13.56 MHz, changes the discharge regime into a uniform glow discharge. A larger discharge gap also opens other options. One method, outlined above, is to increase sheath thickness but if the number of sheath regions are also increased it will produce the same effect. In other words, if the surface area in contact with the plasma is increased, then dissociation reactions will be higher. The addition of beads [27] [28], increases electric field strength especially near intersection points. Hence, one can reduce discharge gap or increase the gap and fill the space with spherical beads. The geometry of the beads may have an effect on the relative increase on the dissociation but is not explored by any study.

- Oxygen ion concentrations were high near the electrodes. Corrosion of the surface due to surface oxidation of copper or aluminum is a risk. This can be avoided by shortening residence times and avoiding significant diffusion towards the electrodes. Similarly, vibrationally excited molecules exist at high temperatures and will further the degradation of reactor walls.

- An applied voltage of 300 V at a frequency of 13.56 MHz, 6.7 cm discharge gap, 1 m^2 electrode area leads to a dissociation of 4.12×10^{-3} % at a very small residence time of 10 μs. The time-averaged total rate of formation of CO from Figure 8 is 7.59×10^{-6} mol/m^3s. Assuming a linear increase in production of CO, it can be said that at a residence time of 1 s, the total moles of CO per unit volume will be 0.759 mol. This is a CO_2 to CO conversion fraction of 0.76, which for a low voltage design and extremely large reactor volume is reasonable.

- Addition of Argon and Xenon at a mole fraction of 0.15 resulted in a significant electron production rate. This can either be used in conjunction with a high voltage to increase the production of electron, or the applied voltage can be relaxed by adding high fractions of Argon. Typically, there is no ideal upper limit for the mole fraction of Argon or Xenon. A larger fraction in combination with a high-pressure flow (atmospheric pressure) will be more economical. For low pressures, less than a few kPa, mole fractions should be kept small, to avoid Argon and Xenon absorbing a larger portion of the applied power. In terms of efficiency, the fraction of power dissipated in ionization reaction of Xenon atoms should be greater than the power absorbed by electron impact CO_2 reactions.

4.9 Zero-Dimensional Modeling

In this section, the Zero-Dimensional model is solved using a reduced CO_2 chemistry presented in [55]. First, the same Helium benchmark model is used to verify that the set of equations deliver acceptable results. Then, the set of reactions for CO_2 are solved. The limitations in assumption for CO_2 modeling are presented and quantified.

1. *Validation of Zero-Dimension kinetics model*

Results obtained from the zero-dimensional model for the benchmark Helium discharge (conditions given in section 4.1) are given in this section. The set of reactions are solved along with some auxiliary equations that enable the calculation of the ambipolar diffusion coefficient and reduced electric field strength. Helium ion mobility is determined from the drift velocity given in [67, 68].

A regression fit was performed to relate reduced electric field strength to ion drift velocity and reduced electric field strength to mean electron energy. Finally, the Einstein relation was used to relate the ambipolar diffusion to mean electron temperature [40]. Table 9 shows the functions.

$$E\mu = v \tag{21}$$

$$D_a \cong \frac{\mu}{e} T_e \quad (22)$$

Where v is the drift velocity in m/s, E is the electric field strength in V/m, μ is the mobility of ions in m^2/Vs, D_a is the ambipolar diffusion coefficient cm^2/s, T_e is the electron temperature in eV and e is the elementary charge.

Table 9. Showing the regression fits and general comments regarding each expression.

Relation	Comments
$v = 0.0166\frac{E}{N} + 0.1609$	$R^2 = 0.9929$
$\frac{E}{N} = 5.6007e^{0.0086\epsilon}$	$R^2 = 0.9846$
$\mu_e = 3\times10^{24}\epsilon^{-0.554}$	$R^2 = 0.9942$. Reduced electron mobility as a function of mean electron energy.
$D_e = 2\times10^{21}\epsilon^{0.4157}$	$R^2 = 0.9983$. Reduced electron diffusion coefficient as a function of mean electron energy.

Table 10 shows the results obtained under the conditions described previously. The electron diffusion loss is computed by accounting for the reflection at the electrodes. Hence, for a reflection coefficient of 0.25, the diffusion losses were multiplied by 0.75.

Table 10. Results from a zero-dimensional model for a Helium CCP.

Pressure	Electron Population (10^{14} cm^{-3})		Mean Electron Energy (eV)	
	Model	Experiment [52]	Model	Experiment [52]
4 Pa (30 mTorr)	2.95	2.80	15.77	9.6
13.3 Pa (100 mTorr)	8.9	12.0	9.1	6.2

40 Pa (300 mTorr)	13.2	23.0	7.5	4.5

The electron population is under-predicted but well within the standard deviation of modeling results by other studies. The mean electron energy is over predicted in all cases but is also within the bounds of similar results in the benchmark study. The mean energy is over predicted most likely because of the omission of other electronically excited states of Helium. The simplified chemistry uses only a single excitation mode which is sufficient to describe the overall behavior.

2. *Zero-Dimensional Modeling Constraints for CO_2*

[55] provides the reaction set that can be used to efficiently model the electron impact dissociation of CO_2 as long as the conversion is below 15%. This model was obtained under certain assumptions. The discharge volume was not the reactor volume (since in a micro-pulse discharge, the electrons are not covering the whole volume uniformly and eject from the dielectric surface based on the local electric field strength) and is in fact much less. In [55], the energy density was multiplied by a factor of seven, which gave good agreement with the experiment. Additionally, a set of dummy reactions were included to incorporate the effect of energy losses due to vibrational excitations.

Table 11. Reaction chemistry from [55]. Electron impact collision cross-sections are different and the sources are presented. All reactions are not shown, only electron impact reactions are given.

CO_2 electron impact cross-sections obtained from [56]	$e + CO_2 \rightarrow 2e + CO_2^+$
	$e + CO_2 \rightarrow e + CO + O$
	$e + CO_2 \rightarrow CO + O^-$
O_2 and O_3 electron impact cross-sections obtained from [69]	$e + O_3 \rightarrow e + O + O_2$
	$e + O_2 \rightarrow e + O + O$

$e + O_2 \rightarrow O^- + O$	
$O + O + M \rightarrow O_2 + M$	(Defined by gas temperature)

Table 12 shows the results obtained for two cases at a residence time of 0.001 seconds and assuming the geometry from [70]. Case A examines the absence of the dummy reactions which leads to notably higher mean energy, this is simply the solution of the reaction set in [55]. The second case (Case B) is obtained by lowering the mean energy by a few electron volts.

The difficulty in properly capturing the discharge profile in a DBD arises from the filamentary nature of the micro discharges. The surface of the dielectric at low frequencies is exposed to several randomly scattered discharges. The exact point where an electron avalanche might strike is dependent on the local electric field strength. If the electric field strength due to charge deposition on the dielectric is low, then a discharge at that spot is less likely to occur [17].

Table 12. Sensitivity of the zero-dimensional model to the mean electron energy. Peak applied voltage of 300 V, maximum discharge current of 0.1 A, average discharge power of 15 W, discharge gap of 2 mm, reactor length of 15 cm and pressure of 5 Pa.

Case	Case A (fixed mean electron energy)		Case B (obtained mean electron energy)	
Mean energy (eV)	3	4	5	4.49
CO_2 Conversion %	0.18	0.182	44.58	18
Electron Number Density (m^{-3})	1.21×10^{16}	1.29×10^{16}	2.48×10^{18}	1.98×10^{18}

The sensitivity of the model to the mean electron energy is high as expected. At a mean energy level, in between 4 to 5 eV, the plasma stabilizes and results are reasonable. If the

energy level is not adjusted either by using a set of invisible reactions that do not alter product chemistry, then dissociation rates are over predicted and results are unreasonable. A similar finding for CO_2 lasers is presented in [71]. The absence of excitation processes can overpredict dissociation rates by 50%.

If the mean energy is over-predicted by a small margin, then electron impact dissociation and attachment proceed fast. Specifically, in the reaction set [55] the production of O^- ion is over estimated and results in further breakdown of CO_2 via an electron detachment reaction. Hence, the effect is non-linear and easily propagates to disturb the mass balance of other species. Since, the reverse reaction of reformation of CO_2 depends only on the bulk gas temperature, it remains unaffected. In this study, the decrease in electron energy is accounted for by reducing the total electron energy by 10%.

From BOLSIG+ the rate constants for a pure CO_2 mixture using the cross-sections from [61], can be obtained to determine approximately the required electron number density equilibrium temperature. If follows from Equation (10), that the time rate of change of electrons ($\frac{\mathrm{dn}}{\mathrm{dt}}$) will be zero when the rate constant for attachment and ionization will be equal. Rearranging Equation (10) to express the right-hand side as a ratio of the rate of ionization to attachment,

$$\frac{\mathrm{dn}}{\mathrm{dt}} = \mathrm{nNk_i}(1-\zeta) \tag{23}$$

Where $\zeta = \frac{k_i}{k_a}$, and k_a is the forward attachment rate constant in $1/m^3s$. Figure 19 shows the change in the ratio with respect to mean electron energies for a reaction set consisting of purely CO_2.

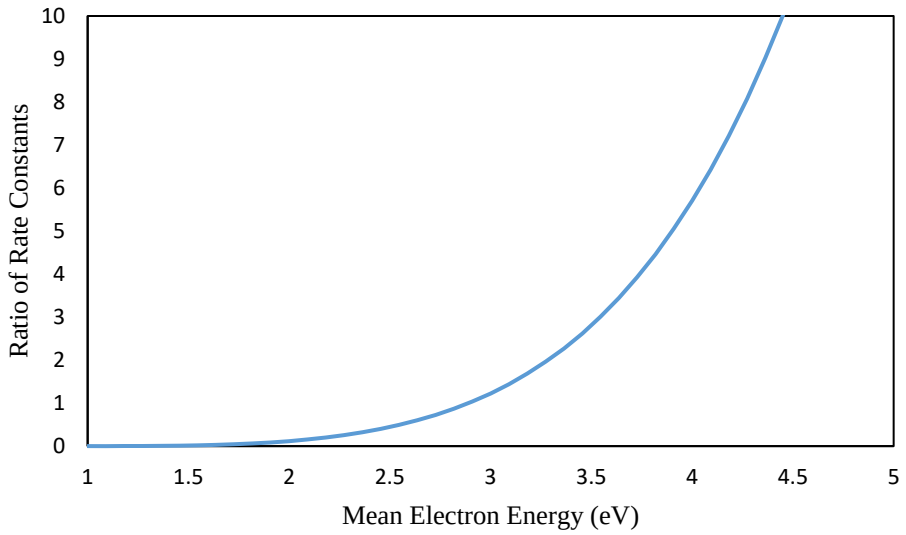

Figure 19. Ratio of ionization and attachment rate constants as a function of mean electron energy for a DBD reactor.

The value of mean electron energy at $\zeta = 1$, is 2.9 eV. This is a good estimate for mean electron energy for DBD plasmas. By reducing the total electron energy by 10% the mean energy (over one RF cycle, since mean electron number density was constant over one cycle) was approximately 2.606 eV using the reduced chemistry set. This lower value is due to other electron loss processes such as dissociative recombination with CO_2. Additionally, from Figure 19, the sensitivity of the solution to model chemistry can be easily observed. If key electron quenching reactions are not properly included, the exponential change in the ratio will greatly overpredict the electron number density leading to erroneous conversion rates. Note that the actual mean electron energy from Equation (11) will differ depending on the applied power density profile. As power supplied to the electrons increases (for an AC signal) ionization rate will increase and attachment rate decrease. Similarly, the balance is maintained during the powering down phase when ionization rate is lower than attachment rate. Hence, the electron equilibrium is established but in a periodic manner.

Table 13 shows characteristic qualitative trends for conversion, electron density and mean electron energy for different reactor volumes. The volume is changed by increasing

reactor length. At higher volumes, power density declines and conversion drops. Note that the residence time was fixed at 0.001 s. Conversion efficiency measures are also give, it is defined by Equation (24)

$$\eta = \frac{\chi \Delta h}{SEI} \tag{24}$$

Where, χ is the conversion of CO_2 to CO, Δh is the enthalpy change of reaction equal to 5.5 eV per molecule of CO_2 and SEI is the specific energy input in J/cm^3

Table 13. Change in Electron density, Mean energy and percentage dissociation of CO_2 as length changes at a residence time of 1 ms and an applied peak power of 30 W (Average power was 15 W).

Length (m)	0.075	0.15	0.3	0.45
CO_2 to CO Conversion %	1.1	0.44	0.17	0.09
Conversion Efficiency %	13	10	8	7
Electron Number Density (m^{-3})	2.14 x10^{17}	1.10 x10^{17}	5.71 x10^{16}	3.92 x10^{16}
Mean Electron Energy (eV)	2.67	2.63	2.56	2.52

The model can clearly capture qualitative trends in the discharge. The quantitative aspect is limited in accuracy. One of the major limitations is that two unique reactor designs with equal discharge volume will give same results under the same conditions. The difference does not appear in the power density, since it is the ratio of applied power to reactor volume. One way to include the difference in designs is to include the diffusion losses towards the walls. Excited species, will transfer excess energy to the walls of the reactor and heat the electrodes or dielectric. The flux to the walls can be obtained by taking into account the characteristic diffusion length and diffusion coefficient of each species.

CCP or MHCD reactors present a unique design for CO_2 dissociation. The loss of electrons due to a conductive surface (electrodes) increase the mean electron energy at that point. Simply, for a given mean total energy, ε, the average energy per electron will

increase if the electron number density is less. The total specific energy input is given to a lesser density which results in more mean energy per electron. This fact is illustrated indirectly in the above model. When the total energy level is lowered, dissociation rates increase.

Using this model CCP and MHCD reactors can be easily studied and diffusion losses can be accounted for and the balance of species will be primarily due to diffusion, which can simplify the model as attachment reactions need not be included for every species, such as oxygen.

Hence, CO_2 dissociation modeling still appears to be case specific. Modifications to the models are required because of simplifications or inherent lack of information that cannot be included such as the discharge volume to reactor volume ratio.

CHAPTER 5

CONCLUSION AND FUTURE WORK

In this study, two analytical techniques are used to model CO_2 dissociation in non-thermal plasma reactors. The first method is a solution to the one-dimensional fluid approximation for two temperature plasma. The spatial distribution of key number densities and generation/loss rates for species such as electrons and carbon monoxide (Synthesis Gas) was obtained in a CCP. The second method is a zero-dimensional kinetics analysis coupled with the solution of the electron energy equation to examine temporal growth of the total species in any reactor. This is used to perform a parametric analysis since dissociation of CO_2 is influenced by applied power, frequency and reactor geometry.

5.1 Summary

The following points summarize the findings of this study.

- The spatial distribution of electrons shows a peak close to the sheath and tends to decay towards the bulk. Since, the boundary conditions were symmetric, the solution was symmetric about the midpoint of the reactor. The dominant species responsible for charge neutrality was the CO_2^+ ion. If Ar or Xe is injected in small concentrations, the primary ion balance is maintained by Ar^+ or Xe^+ together with CO_2^+.

- Reaction rate profiles were distributed similarly but differed in either being wholly dominated by sheath temperatures or electron density. Attachment reaction peaks are closer to the electron density peak, displaying that the rate is affected more by number density than by high mean energy, whereas ionization dissociation reactions were entirely dominated by the sheath region. This suggests that a higher electron number density, commonly found in DBD reactors will favor attachment dissociation. Nearly, all reaction rates decreased to a small value (close to zero) in

the neutral region. Since, the mean temperature was low 1 to 3 eV all rates are suppressed with an exception of vibrational reaction rates.

- The increase in voltage from 300 to 800 V in the one-dimensional simulations did not change the bulk temperature profile but augmented reactions rates in the sheath.

5.2 Conclusions

The following conclusions can be drawn from this study.

- It is concluded that because CO generation rates are low in the equilibrium region, designs where discharge gaps are smaller compared to reactor length are more feasible. Additionally, the use of beads and dielectrics that enhance local electric field strengths will improve dissociation, by raising electron temperatures in the bulk. Increasing the applied voltage also increases the dissociation rate but is significant only in the sheath regions. The thickness of the sheath increases as voltage is increased.

- The use of noble gases such as Argon, Helium and Xenon enhances CO_2 ionization rate and changes the distribution of the electron density. There is a marked increase in electron density in the bulk but a relatively lower increase close to the sheath. Recommended concentrations are less than 50 %.

- The use of one-dimensional models to study dissociation under long residence times is prohibitive as even simple models such as the one examined in this study can take several hours to compute. It is preferable to use the zero-dimensional kinetics analysis with a detailed chemistry to study the bulk effects, such as species growth and energy variation.

- The zero-dimensional model is sensitive to the choice of chemical reactions and respective collision cross-section, in the case of electron impact reactions. The computation time is significantly faster and yields results with reasonable

accuracy. For designing a reactor, it is recommended to simulate input parameters and geometry using a Zero-Dimensional model first and optimize using a 1-D or 2-D fluid simulation.

5.3 Future Work

There is significant effort still needed both experimentally and numerically to properly compose a model that can quantify CO_2 dissociation without assumptions that render the model case specific. A benchmarking study needs to be conducted, similar to that of Helium with a simple geometry to first obtain a validated physical model. This can be later extended to incorporate the specific effects of the discharge.

For an optimal design, higher voltage setting and a higher frequency such as a RF signal is recommended. CO_2 breakdown can be increased by lowering discharge gap, increasing voltage and introducing a buffer gas such as Argon or Xenon to increase ionization and electron impact collisions leading to dissociation. For higher flow rates, a longer reactor is desirable but the length to discharge gap ratio should be carefully chosen to avoid low power densities. The zero-dimensional kinetics model with reduced chemistry can provide good estimates for initial design parameters. Model chemistry, however, has to be carefully selected to ensure key reactions are not omitted to avoid erroneous results.

REFERENCES

[1] J. A. Duffie and W. A. Beckman, "Solar engineering of thermal processes," 1980.

[2] S. Mahammadunnisa, E. L. Reddy, D. Ray, C. Subrahmanyam and J. C. Whitehead, "CO 2 reduction to syngas and carbon nanofibres by plasma-assisted in situ decomposition of water," *International Journal of Greenhouse Gas Control*, vol. 16, pp. 361-363, 2013.

[3] W. Bongers, S. Welzel, D. van den Bekerom, G. Frissen, G. van Rooij, A. Goede, M. Graswinckel, P. Groen, N. den Harder, B. van Heemert and others, "Developments in CO2 dissociation using non-equilibrium microwave plasma activation for solar fuels," in *ISPC 2015, 22nd International Symposium on Plasma Chemistry*, 2015.

[4] W. Bongers, H. Bouwmeester, B. Wolf, F. Peeters, S. Welzel, D. van den Bekerom, N. den Harder, A. Goede, M. Graswinckel, P. W. Groen and others, "Plasma-driven dissociation of CO2 for fuel synthesis," *Plasma Processes and Polymers*, 2016.

[5] A. P. Goede, W. A. Bongers, M. F. Graswinckel, R. M. van de Sanden, M. Leins, J. Kopecki, A. Schulz and M. Walker, "Production of solar fuels by CO2 plasmolysis," in *EPJ Web of Conferences*, 2014.

[6] V. Rusanov, A. Fridman and G. Sholin, "The physics of a chemically active plasma with nonequilibrium vibrational excitation of molecules," *Physics-Uspekhi*, vol. 24, no. 6, pp. 447-474, 1981.

[7] S. Samukawa, M. Hori, S. Rauf, K. Tachibana, P. Bruggeman, G. Kroesen, J. C. Whitehead, A. B. Murphy, A. F. Gutsol, S. Starikovskaia and others, "The 2012 plasma roadmap," *Journal of Physics D: Applied Physics*, vol. 45, no. 25, p. 253001, 2012.

[8] I. Rafatov, D. Akbar and S. Bilikmen, "Modelling of non-uniform DC driven glow discharge in argon gas," *Physics Letters A*, vol. 367, no. 1, pp. 114-119, 2007.

[9] T. Paulmier and L. Fulcheri, "Use of non-thermal plasma for hydrocarbon reforming," *Chemical engineering journal*, vol. 106, no. 1, pp. 59-71, 2005.

[10] H. L. Chen, H. M. Lee, S. H. Chen, Y. Chao and M. B. Chang, "Review of plasma catalysis on hydrocarbon reforming for hydrogen production—interaction,

integration, and prospects," *Applied Catalysis B: Environmental,* vol. 85, no. 1, pp. 1-9, 2008.

[11] Y.-C. Yang, B.-J. Lee and Y.-N. Chun, "Characteristics of methane reforming using gliding arc reactor," *Energy,* vol. 34, no. 2, pp. 172-177, 2009.

[12] Q. Wang, B. Spasova, V. Hessel and G. Kolb, "Methane reforming in a small-scaled plasma reactor--industrial application of a plasma process from the viewpoint of the environmental profile," *Chemical Engineering Journal,* vol. 262, pp. 766-774, 2015.

[13] B. Zhu, X.-S. Li, J.-L. Liu, X. Zhu and A.-M. Zhu, "Kinetics study on carbon dioxide reforming of methane in kilohertz spark-discharge plasma," *Chemical Engineering Journal,* vol. 264, pp. 445-452, 2015.

[14] B. Zhu, X.-S. Li, J.-L. Liu and A.-M. Zhu, "Optimized mixed reforming of biogas with O 2 addition in spark-discharge plasma," *international journal of hydrogen energy,* vol. 37, no. 22, pp. 16916-16924, 2012.

[15] B. Zhu, X.-S. Li, C. Shi, J.-L. Liu, T.-L. Zhao and A.-M. Zhu, "Pressurization effect on dry reforming of biogas in kilohertz spark-discharge plasma," *international journal of hydrogen energy,* vol. 37, no. 6, pp. 4945-4954, 2012.

[16] T. Nunnally, K. Gutsol, A. Rabinovich, A. Fridman, A. Gutsol and A. Kemoun, "Dissociation of CO2 in a low current gliding arc plasmatron," *Journal of Physics D: Applied Physics,* vol. 44, no. 27, p. 274009, 2011.

[17] B. Eliasson, W. Egli and U. Kogelschatz, "Modelling of dielectric barrier discharge chemistry," *Pure and applied chemistry,* vol. 66, no. 6, pp. 1275-1286, 1994.

[18] V. Goujard, J.-M. Tatibou{\"e}t and C. Batiot-Dupeyrat, "Use of a non-thermal plasma for the production of synthesis gas from biogas," *Applied Catalysis A: General,* vol. 353, no. 2, pp. 228-235, 2009.

[19] M. Pham, V. Goujard, J. Tatibouet and C. Batiot-Dupeyrat, "Activation of methane and carbon dioxide in a dielectric-barrier discharge-plasma reactor to produce hydrocarbons—Influence of La 2 O 3/γ-Al 2 O 3 catalyst," *Catalysis today,* vol. 171, no. 1, pp. 67-71, 2011.

[20] C. Shin, "Dissociation of carbon dioxide in an Al/Al2O3 microchannel plasma reactor at atmospheric pressure," 2015.

[21] N. A. S. Amin and others, "Co-generation of synthesis gas and C 2+ hydrocarbons from methane and carbon dioxide in a hybrid catalytic-plasma reactor: a review," *Fuel,* vol. 85, no. 5, pp. 577-592, 2006.

[22] Z. Bo, J. Yan, X. Li, Y. Chi and K. Cen, "Plasma assisted dry methane reforming using gliding arc gas discharge: effect of feed gases proportion," *International Journal of Hydrogen Energy,* vol. 33, no. 20, pp. 5545-5553, 2008.

[23] X. Duan, Y. Li, W. Ge and B. Wang, "Degradation of CO2 through dielectric barrier discharge microplasma," *Greenhouse Gases: Science and Technology,* vol. 5, no. 2, pp. 131-140, 2015.

[24] A. Yamamoto, S. Mori and M. Suzuki, "Scale-up or numbering-up of a micro plasma reactor for the carbon dioxide decomposition," *Thin solid films,* vol. 515, no. 9, pp. 4296-4300, 2007.

[25] G. Petitpas, J.-D. Rollier, A. Darmon, J. Gonzalez-Aguilar, R. Metkemeijer and L. Fulcheri, "A comparative study of non-thermal plasma assisted reforming technologies," *International Journal of Hydrogen Energy,* vol. 32, no. 14, pp. 2848-2867, 2007.

[26] A. Ozkan, T. Dufour, G. Arnoult, P. De Keyzer, A. Bogaerts and F. Reniers, "CO 2--CH 4 conversion and syngas formation at atmospheric pressure using a multi-electrode dielectric barrier discharge," *Journal of CO2 utilization,* vol. 9, pp. 74-81, 2015.

[27] C. De Bie, B. Verheyde, T. Martens, J. van Dijk, S. Paulussen and A. Bogaerts, "Fluid modeling of the conversion of methane into higher hydrocarbons in an atmospheric pressure dielectric barrier discharge," *Plasma Processes and Polymers,* vol. 8, no. 11, pp. 1033-1058, 2011.

[28] C. De Bie, J. van Dijk and A. Bogaerts, "The dominant pathways for the conversion of methane into oxygenates and syngas in an atmospheric pressure dielectric barrier discharge," *The Journal of Physical Chemistry C,* vol. 119, no. 39, pp. 22331-22350, 2015.

[29] D. Mei, X. Zhu, Y.-L. He, J. D. Yan and X. Tu, "Plasma-assisted conversion of CO2 in a dielectric barrier discharge reactor: understanding the effect of packing materials," *Plasma Sources Science and Technology,* vol. 24, no. 1, p. 015011, 2014.

[30] C.-j. Liu, G.-h. Xu and T. Wang, "Non-thermal plasma approaches in CO 2 utilization," *Fuel Processing Technology,* vol. 58, no. 2, pp. 119-134, 1999.

[31] M. Babaie, P. Davari, P. Talebizadeh, F. Zare, H. Rahimzadeh, Z. Ristovski and R. Brown, "Performance evaluation of non-thermal plasma on particulate matter, ozone and CO 2 correlation for diesel exhaust emission reduction," *Chemical Engineering Journal*, vol. 276, pp. 240-248, 2015.

[32] D. Yap, J.-M. Tatibou{\"e}t and C. Batiot-Dupeyrat, "Carbon dioxide dissociation to carbon monoxide by non-thermal plasma," *Journal of CO2 Utilization*, vol. 12, pp. 54-61, 2015.

[33] D. B. Nguyen and W. G. Lee, "Comparison of different applied voltage waveforms on CO2 reforming of CH4 in an atmospheric plasma system," *Korean Journal of Chemical Engineering*, vol. 32, no. 1, pp. 62-67, 2015.

[34] G. Hagelaar and L. Pitchford, "Solving the Boltzmann equation to obtain electron transport coefficients and rate coefficients for fluid models," *Plasma Sources Science and Technology*, vol. 14, no. 4, p. 722, 2005.

[35] A. Bogaerts, Mathematical modeling of a direct current glow discharge in argon, Universitaire Instelling Antwerpen, 1996.

[36] P. M. Bellan, Fundamentals of plasma physics, Cambridge University Press, 2008.

[37] M. Mitchner and C. H. Kruger, Partially ionized gases, vol. 8, Wiley New York, 1973.

[38] M. Lietzke and C. Mullins, "The thermal decomposition of carbon dioxide," *Journal of Inorganic and Nuclear Chemistry*, vol. 43, no. 8, pp. 1769-1771, 1981.

[39] A. Fridman, Plasma chemistry, Cambridge university press, 2008.

[40] A. Fridman and L. A. Kennedy, Plasma physics and engineering, CRC press, 2004.

[41] A. Bogaerts, T. Koz{\'a}k, K. van Laer and R. Snoeckx, "Plasma-based conversion of CO 2: current status and future challenges," *Faraday discussions*, vol. 183, pp. 217-232, 2015.

[42] D. B. Graves, "Fluid model simulations of a 13.56-MHz rf discharge: Time and space dependence of rates of electron impact excitation," *Journal of applied physics*, vol. 62, no. 1, pp. 88-94, 1987.

[43] D. P. Lymberopoulos and D. J. Economou, "Fluid simulations of glow discharges: Effect of metastable atoms in argon," *Journal of applied physics,* vol. 73, no. 8, pp. 3668-3679, 1993.

[44] D. Levko and L. L. Raja, "Electron kinetics in atmospheric-pressure argon and nitrogen microwave microdischarges," *Journal of Applied Physics,* vol. 119, no. 16, p. 163303, 2016.

[45] G. Hagelaar and G. Kroesen, "Speeding up fluid models for gas discharges by implicit treatment of the electron energy source term," *Journal of Computational Physics,* vol. 159, no. 1, pp. 1-12, 2000.

[46] G. J. M. Hagelaar, Modeling of microdischarges for display technology, Technische Universiteit Eindhoven, 2000.

[47] L. R. Petzold and others, "A description of DASSL: A differential/algebraic system solver," in *Proc. IMACS World Congress*, 1982.

[48] L. V. Fausett, Applied Numerical Analysis Using MATLAB (2Nd Edition), Upper Saddle River, NJ, USA: Prentice-Hall, Inc., 2007.

[49] K. G. Marchand, "Computational model of one-dimensional dielectric barrier discharges," 2005.

[50] C. M. Snowden, Introduction to semiconductor device modelling, World Scientific, 1986.

[51] R. Aerts, T. Martens and A. Bogaerts, "Influence of vibrational states on CO2 splitting by dielectric barrier discharges," *The Journal of Physical Chemistry C*, vol. 116, no. 44, pp. 23257-23273, 2012.

[52] M. Surendra, "Radiofrequency discharge benchmark model comparison," *Plasma Sources Science and Technology,* vol. 4, no. 1, p. 56, 1995.

[53] L. F. Spencer and A. D. Gallimore, "Efficiency of CO2 dissociation in a radio-frequency discharge," *Plasma Chemistry and Plasma Processing,* vol. 31, no. 1, pp. 79-89, 2011.

[54] L. Spencer and A. Gallimore, "CO2 dissociation in an atmospheric pressure plasma/catalyst system: a study of efficiency," *Plasma Sources Science and Technology,* vol. 22, no. 1, p. 015019, 2012.

[55] R. Aerts, W. Somers and A. Bogaerts, "Carbon dioxide splitting in a dielectric barrier discharge plasma: a combined experimental and computational study," *ChemSusChem,* vol. 8, no. 4, pp. 702-716, 2015.

[56] Y. Itikawa and others, "Cross sections for electron collisions with carbon dioxide," *Journal of Physical and Chemical Reference Data,* vol. 31, no. 3, pp. 749-768, 2002.

[57] J. Shin and L. L. Raja, "Dynamics of pulse phenomena in helium dielectric-barrier atmospheric-pressure glow discharges," *Journal of applied physics,* vol. 94, no. 12, pp. 7408-7415, 2003.

[58] T. Kozak, "Splitting of CO2 by vibrational excitation in non-equilibrium plasmas: a reaction kinetics model".

[59] T. Kozak and A. Bogaerts, "Evaluation of the energy efficiency of CO2 conversion in microwave discharges using a reaction kinetics model," *Plasma Sources Science and Technology,* vol. 24, no. 1, p. 015024, 2014.

[60] S. Ponduri, M. Becker, S. Welzel, M. van de Sanden, D. Loffhagen and R. Engeln, "Fluid modelling of CO2 dissociation in a dielectric barrier discharge," *Journal of Applied Physics,* vol. 119, no. 9, p. 093301, 2016.

[61] J. Lowke, A. Phelps and B. Irwin, "Predicted electron transport coefficients and operating characteristics of CO2--N2--He laser mixtures," *Journal of Applied Physics,* vol. 44, no. 10, pp. 4664-4671, 1973.

[62] O. Taylan and H. Berberoglu, "Dissociation of carbon dioxide using a microhollow cathode discharge plasma reactor: effects of applied voltage, flow rate and concentration," *Plasma Sources Science and Technology,* vol. 24, no. 1, p. 015006, 2014.

[63] X. Yuan and L. L. Raja, "Computational study of capacitively coupled high-pressure glow discharges in helium," *IEEE Transactions on Plasma Science,* vol. 31, no. 4, pp. 495-503, 2003.

[64] X. Yuan and L. L. Raja, "Role of trace impurities in large-volume noble gas atmospheric-pressure glow discharges," *Applied physics letters,* vol. 81, no. 5, pp. 814-816, 2002.

[65] A. Phelps, "Cross sections and swarm coefficients for nitrogen ions and neutrals in N2 and argon ions and neutrals in Ar for energies from 0.1 eV to 10 keV," *Journal of Physical and Chemical Reference Data,* vol. 20, no. 3, pp. 557-573, 1991.

[66] M. Ramakers, I. Michielsen, R. Aerts, V. Meynen and A. Bogaerts, "Effect of argon or helium on the CO2 conversion in a dielectric barrier discharge," *Plasma Processes and Polymers,* vol. 12, no. 8, pp. 755-763, 2015.

[67] M. A. Biondi and S. C. Brown, "Measurements of ambipolar diffusion in helium," *Physical Review,* vol. 75, no. 11, p. 1700, 1949.

[68] R. Golyatina and S. Maiorov, "Dependence of characteristics of helium ion diffusion and drift in own gas on its temperature," *Bulletin of the Lebedev Physics Institute,* vol. 39, no. 7, pp. 208-213, 2012.

[69] J. McConkey, C. Malone, P. Johnson, C. Winstead, V. McKoy and I. Kanik, "Electron impact dissociation of oxygen-containing molecules--A critical review," *Physics Reports,* vol. 466, no. 1, pp. 1-103, 2008.

[70] S. Paulussen, B. Verheyde, X. Tu, C. De Bie, T. Martens, D. Petrovic, A. Bogaerts and B. Sels, "Conversion of carbon dioxide to value-added chemicals in atmospheric pressure dielectric barrier discharges," *Plasma Sources Science and Technology,* vol. 19, no. 3, p. 034015, 2010.

[71] A. Cenian, A. Chernukho and V. Borodin, "Modeling of Plasma-Chemical Reactions in Gas Mixture of CO2 lasers. II. Theoretical Model and its Verification," *Contributions to Plasma Physics,* vol. 35, no. 3, pp. 273-296, 1995.

[72] J. Van Dijk, G. Kroesen and A. Bogaerts, "Plasma modelling and numerical simulation," *Journal of Physics D: Applied Physics,* vol. 42, no. 19, p. 190301, 2009.

[73] P. Scheubert and others, Modelling and diagnostics of low pressure plasma discharges, Shaker, 2002.

[74] D. Ray and C. Subrahmanyam, "CO 2 decomposition in a packed DBD plasma reactor: influence of packing materials," *RSC Advances,* vol. 6, no. 45, pp. 39492-39499, 2016.

[75] L. D. Pietanza, G. Colonna, V. Laporta, R. Celiberto, G. D'Ammando, A. Laricchiuta and M. Capitelli, "Influence of Electron Molecule Resonant Vibrational Collisions over the Symmetric Mode and Direct Excitation-Dissociation Cross Sections of CO2 on the Electron Energy Distribution Function and Dissociation Mechanisms in Cold Pure CO2 Plasmas," *The Journal of Physical Chemistry A,* vol. 120, no. 17, pp. 2614-2628, 2016.

[76] M. Moreau, N. Orange and M. Feuilloley, "Non-thermal plasma technologies: new tools for bio-decontamination," *Biotechnology advances,* vol. 26, no. 6, pp. 610-617, 2008.

[77] R. McAdams, "Prospects for non-thermal atmospheric plasmas for pollution abatement," *Journal of Physics D: Applied Physics,* vol. 34, no. 18, p. 2810, 2001.

[78] R. Marriott, "Molecular collision cross sections and vibrational relaxation in carbon dioxide," *Proceedings of the Physical Society,* vol. 84, no. 6, p. 877, 1964.

[79] R. Locht and M. Davister, "The dissociative electroionization of carbon dioxide by low-energy electron impact. The C+, O+ and CO+ dissociation channels," *International journal of mass spectrometry and ion processes,* vol. 144, no. 1, pp. 105-129, 1995.

[80] A. Lebouvier, S. A. Iwarere, P. d'Argenlieu, D. Ramjugernath and L. Fulcheri, "Assessment of carbon dioxide dissociation as a new route for syngas production: a comparative review and potential of plasma-based technologies," *Energy \& Fuels,* vol. 27, no. 5, pp. 2712-2722, 2013.

[81] H.-H. Kim, "Nonthermal plasma processing for air-pollution control: a historical review, current issues, and future prospects," *Plasma Processes and Polymers,* vol. 1, no. 2, pp. 91-110, 2004.

[82] B. Jiang and H. Guo, "Communication: Enhanced dissociative chemisorption of CO2 via vibrational excitation," *The Journal of chemical physics,* vol. 144, no. 9, p. 091101, 2016.

[83] M. Jafarbegloo, A. Tarlani, A. W. Mesbah and S. Sahebdelfar, "Thermodynamic analysis of carbon dioxide reforming of methane and its practical relevance," *International Journal of Hydrogen Energy,* vol. 40, no. 6, pp. 2445-2451, 2015.

[84] Y. Itikawa, "Cross sections for electron collisions with oxygen molecules," *Journal of Physical and Chemical Reference Data,* vol. 38, no. 1, pp. 1-20, 2009.

[85] Y. Itikawa, "Cross Sections for Electron Collisions with Carbon Monoxide," *Journal of Physical and Chemical Reference Data,* vol. 44, no. 1, p. 013105, 2015.

[86] A. Indarto, D. R. Yang, J.-W. Choi, H. Lee and H. K. Song, "Gliding arc plasma processing of CO 2 conversion," *Journal of hazardous materials,* vol. 146, no. 1, pp. 309-315, 2007.

[87] G. Horvath, J. Skaln{\`y} and N. Mason, "FTIR study of decomposition of carbon dioxide in dc corona discharges," *Journal of Physics D: Applied Physics,* vol. 41, no. 22, p. 225207, 2008.

[88] W. Hoeben, E. van Heesch, F. Beckers, W. Boekhoven and A. Pemen, "Plasma-Driven Water Assisted CO 2 Methanation," *IEEE Transactions on Plasma Science,* vol. 43, no. 6, pp. 1954-1958, 2015.

[89] J. Greg{\'o}rio, C. Boisse-Laporte and L. L. Alves, "Fast Time-Relaxation Algorithm to Solve Plasma Fluid Equations," *IEEE Transactions on Plasma Science,* vol. 38, no. 9, p. 2312, 2010.

[90] A. Ghorbanzadeh, R. Lotfalipour and S. Rezaei, "Carbon dioxide reforming of methane at near room temperature in low energy pulsed plasma," *international journal of hydrogen energy,* vol. 34, no. 1, pp. 293-298, 2009.

[91] D. Rapp and D. D. Briglia, "Total Cross Sections for Ionization and Attachment in Gases by Electron Impact. II. Negative-Ion Formation," *The Journal of Chemical Physics,* vol. 43, no. 5, pp. 1480-1489, 1965.